

Supporting Information

Highly Selective and Sensitive Fluorescence Detection of Zn²⁺ and Cd²⁺ Ions by an Acridine Sensor

Arne Visscher, Sebastian Bachmann, Christoph Schnegelsberg,[†] Thorsten Teuteberg,[‡] Ricardo Mata,[‡] and Dietmar Stalke*

Institut für Anorganische Chemie der Universität Göttingen, Tammannstraße 4, 37077 Göttingen, Germany

[†] Institut für Organische und Biomolekulare Chemie der Universität Göttingen, Tammannstraße 2, 37077 Göttingen, Germany.

[‡] Institut für Physikalische Chemie der Universität Göttingen, Tammannstraße 6, 37077 Göttingen, Germany.

* dstalke@chemie.uni-goettingen.de

Table of content

1. General considerations	2
2. Synthesis procedures	3
3. NMR spectra	5
4. UV/vis absorption spectra	17
5. Fluorescence spectra	18
6. Mass spectra	20
7. Crystallographic data	23
8. Computational studies	29
9. References	31

1. General considerations

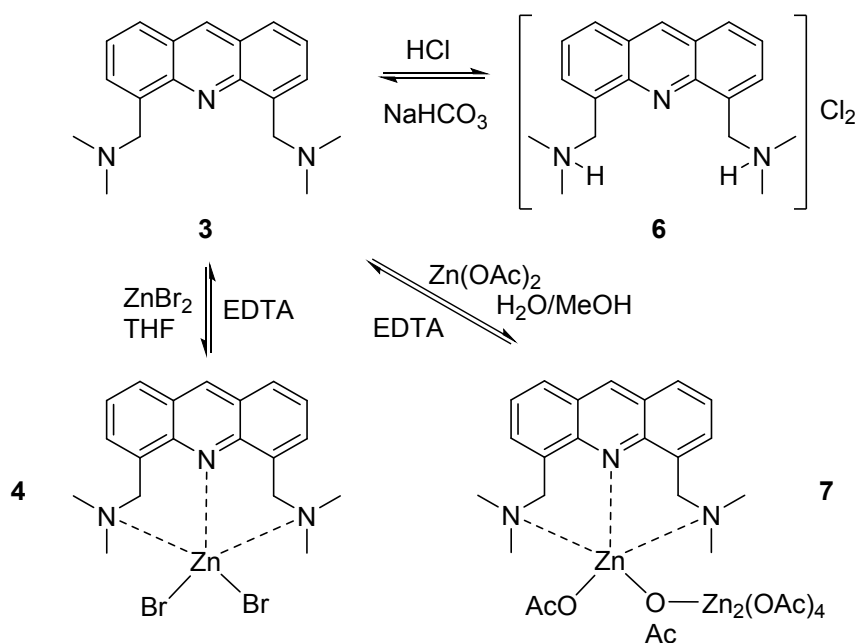
Materials and measurements. All materials were purchased from SIGMA-ALDRICH, VWR INTERNATIONAL, and ABCR CHEMICALS and used without further purification – except water which was purified first through a Millipore water purification system Milli-RO 3 plus and finally with a Millipore ultrapure water system Milli-Q plus 185. The NMR measurements were done on a BRUKER Avance 300 and BRUKER Avance III HD 400 spectrometer. Unless stated otherwise, all NMR experiments were done at 298 K. The chemical shifts (δ) are reported in parts per million (ppm) relative to the residual proton signals of the incomplete deuterated solvents. Absorption spectra (UV/vis) for **2** were recorded at a JASCO V-650 double beam spectrophotometer and for **3** at an AGILENT 8453 diode array spectrophotometer. The fluorescence measurements were carried out on a HORIBA JOBIN-YVON Fluoromax-4 spectrometer. Compound **2** and **3** were dissolved either in methanol or dichloromethane with a concentration of $1 \cdot 10^{-5}$ M. The metal salts contained only bromides as anions. All emission spectra were recorded with an excitation wavelength of 357 nm. For electrospray ionization mass spectrometric studies, sample solutions of $c \approx 5$ mM were continuously administered into the ESI source of a micrOTOF-Q II mass spectrometer (BRUKER DALTONIK) by a step motor-driven gas-tight syringe (flow rate: 0.5 ml/h). This instrument combines a quadrupole mass filter with a time-of-flight analyzer. The simulated isotope patterns were calculated using the COMPASS software package from BRUKER DALTONIK.

Single-Crystal Structural Analysis. Suitable single crystals for X-ray structural analysis were selected from a Schlenk flask under an argon atmosphere and covered with perfluorated polyether oil on a microscope slide, which was cooled with a nitrogen gas flow using the X-TEMP2 device.¹ An appropriate crystal was selected using a polarizing microscope, mounted on the tip of a MiTeGen MicroMount, fixed to a goniometer head and shock-cooled by the crystal cooling device. The dataset for **4a** was collected on an INCOATEC Mo microsource² with mirror optics and a Mo- K_α radiation with $\lambda = 71.073$ pm. The data for **5** and **7** were collected at an INCOATEC Ag microfocuss source with INCOATEC Quazar mirror optics and an Ag radiation with $\lambda = 56.086$ pm. Both diffractometers were equipped with an APEX II detector with a D8 goniometer and a lowtemperature device. The dataset for **6** was recorded using Cu- K_α radiation ($\lambda = 154.178$ pm) on a Bruker MacScience rotating anode diffractometer equipped with a SMART6000 CCD detector. The data for **4a** – **7** were integrated with SAINT³ and an empirical absorption correction (SADABS)⁴ was applied. The structures were solved by direct methods using SHELXT⁵ and refined by full-matrix least-squares methods against F^2 (SHELXL)⁶ within the SHELXLE GUI.⁷ Unless stated otherwise, the hydrogen atoms were refined isotropically on calculated positions using a riding model with their U_{iso} values constrained to equal 1.5 times the U_{eq} of their pivot atoms for terminal sp^3 carbon atoms and 1.2 times for all other carbon atoms. Disordered moieties were refined using bond length restraints and anisotropic displacement parameter restraints.⁸ Crystallographic data for the structures reported in this paper have been deposited within the Cambridge Crystallographic Data Centre. The CCDC numbers, crystal data, and experimental details for the X-ray measurements are listed in Table S7.2 of this supplement. Copies of the data can be obtained free of charge from the Cambridge Crystallographic Data Centre via www.ccdc.cam.ac.uk/data_request/cif or from the corresponding author.

Computational studies. All geometry optimizations were carried out at the B3LYP-D3/def2-TZVPP⁹ level of theory (including Becke-Jones type damping¹⁰ of the dispersion correction^{9f}). In the case of Cd, the Stuttgart/Dresden ECP28MDF¹¹ was used. The electronic densities and the corresponding NBO analysis¹² were computed at the same level. All calculations were carried out with the ORCA¹³ program package. The B3LYP calculations were performed under the RIJCOSX approximation¹⁴.

2. Synthesis procedures

Scheme S1: Reaction pathways to the metal ion complexes (**4**, **7**) and the hydrochlorinated species (**6**) as well as their back reactions to **3**.



Synthesis of 4,5-bis(N,N-dimethylaminemethylene)acridine hydrochloride (6): Conc. HCl (0.4 ml, 4.8 mmol, 4.8 eq) was added dropwise to a solution of **3** (293 mg, 1.00 mmol, 1.0 eq) in toluene (15 ml). After stirring for 15 min at rt, a dark yellow precipitate was formed which was filtered and washed with toluene (3x 5 ml). The pure product (342 mg, 934 μmol , 93.4%) was dried under reduced pressure to obtain a bright yellow powder. Suitable crystals for X-ray analysis were formed after a recrystallization from methanol. ^1H NMR (300 MHz, DMSO-d_6): δ 10.42 (s, 2 H, NH), 9.36 (s, 1 H, H_9), 8.38 (d, $^3J = 8.2$ Hz, 2 H, $\text{H}_{1,8}$), 8.17 (d, $^3J = 6.4$ Hz, 2 H, $\text{H}_{3,6}$), 7.77 (dd, $^3J = 8.2, 7.0$ Hz, 2 H, $\text{H}_{2,7}$), 5.16 (d, $^3J = 5.7$ Hz, 2 H, CH_2), 2.91 (d, $^3J = 4.8$ Hz, 12 H, CH_3). $^{13}\text{C}\{^1\text{H}\}$ NMR (75 MHz, DMSO-d_6): δ 146.1 (2 C, $\text{C}_{4a,10a}$), 138.6 (1 C, C_9), 135.8 (2 C, $\text{C}_{3,6}$), 131.2 (2 C, $\text{C}_{1,8}$), 128.1 (2 C, $\text{C}_{4,5}$), 126.5 (2 C, $\text{C}_{8a,9a}$), 125.7 (2 C, $\text{C}_{2,7}$), 55.9 (2 C, CH_2), 42.5 (4 C, CH_3). ESI-MS: m/z (%) 400 (27) $[\text{M}+\text{Cl}]^-$, 364 (18) $[\text{M}-\text{H}]^-$. Anal. Calcd for $\text{C}_{19}\text{H}_{25}\text{N}_3\text{Cl}_2$: C, 62.29; H, 6.88; N, 11.47; Cl, 19.36. Found: C, 61.46; H, 6.61; N, 11.18; Cl, 20.35.

Synthesis of 4,5-bis(dimethylaminemethylene)acridine (3): Procedure A: The deprotonation of **6** (235 mg, 641 μmol , 1.0 eq) was done in a saturated aqueous NaHCO_3 solution (10 ml, 11.4 mmol, 17.8 eq) which was stirred for 30 min. The product was extracted with ethyl acetate (20 ml) and the organic phase was washed with aqueous NaHCO_3 solution (2x 10 ml). The organic phase was dried with MgSO_4 , filtered and the volatile compounds were removed under reduced pressure. **3** (155 mg, 528 μmol , 82.4%) could be reobtained as a yellow-brown solid.

Procedure B: **4** (139 mg, 268 μmol , 1.0 eq) was suspended in an aq. NaHCO_3 solution (5%, 10 ml) when $\text{Na}_2\text{H}_2\text{EDTA}$ (360 mg, 1.07 mmol, 4 eq), dissolved in an aq. NaHCO_3 solution (10%, 6 ml), was added. The suspension was stirred at room temperature for 45 min. The product was extracted with ethyl acetate (2x 4 ml) and the gathered organic phases were washed with an aq. saturated NaHCO_3 solution (3x 10 ml). The organic phases were dried with MgSO_4 and filtered. After the solvent was removed under reduced pressure, **3** (74 mg, 252 μmol , 94%) was reobtained as a yellow-brown solid.

Crystallization of 4,5-bis(dimethylaminemethylene)acridine tetrakis(μ -acetate) bis(acetate) zinc(II) (7): Anhydrous zinc acetate (100 mg, 545 μ mol, 1.6 eq) was dissolved in dem. water (0.5 ml) and added to a solution of **3** (100 mg, 341 μ mol, 1.0 eq) in methanol. The volatile compounds of the resulting suspension was removed in vacuo and a mixture of toluene with DMF was used to dissolve the product at room temperature. Suitable crystals for X-ray analysis were formed at -30 °C after 10 days.

The free ligand (**3**) could be reobtained by the application of *procedure B* to **7**. A direct yield can not be reported since **7** was not completely isolated before. Nevertheless, 78% (78 mg, 266 μ mol) of the used ligand **3** was gained back.

3. NMR spectra

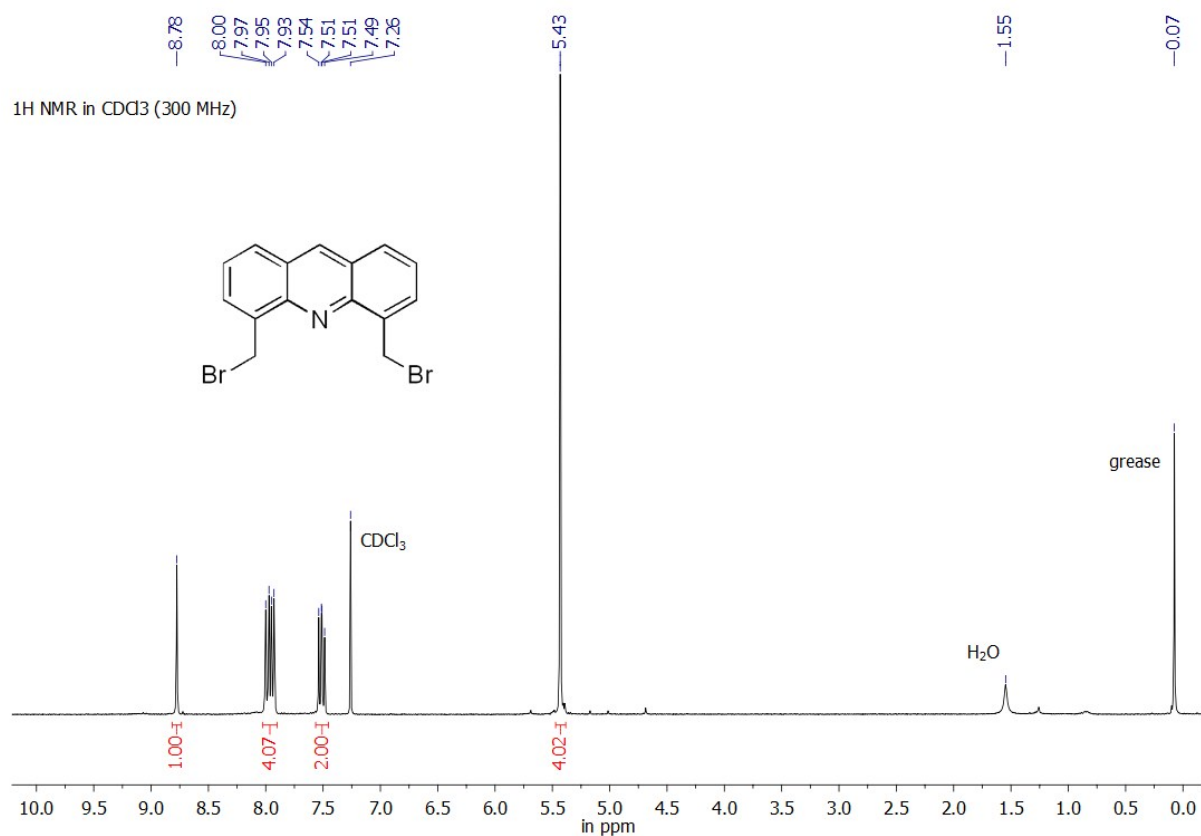


Figure S3.1: ¹H NMR spectrum of **1** in CDCl₃.

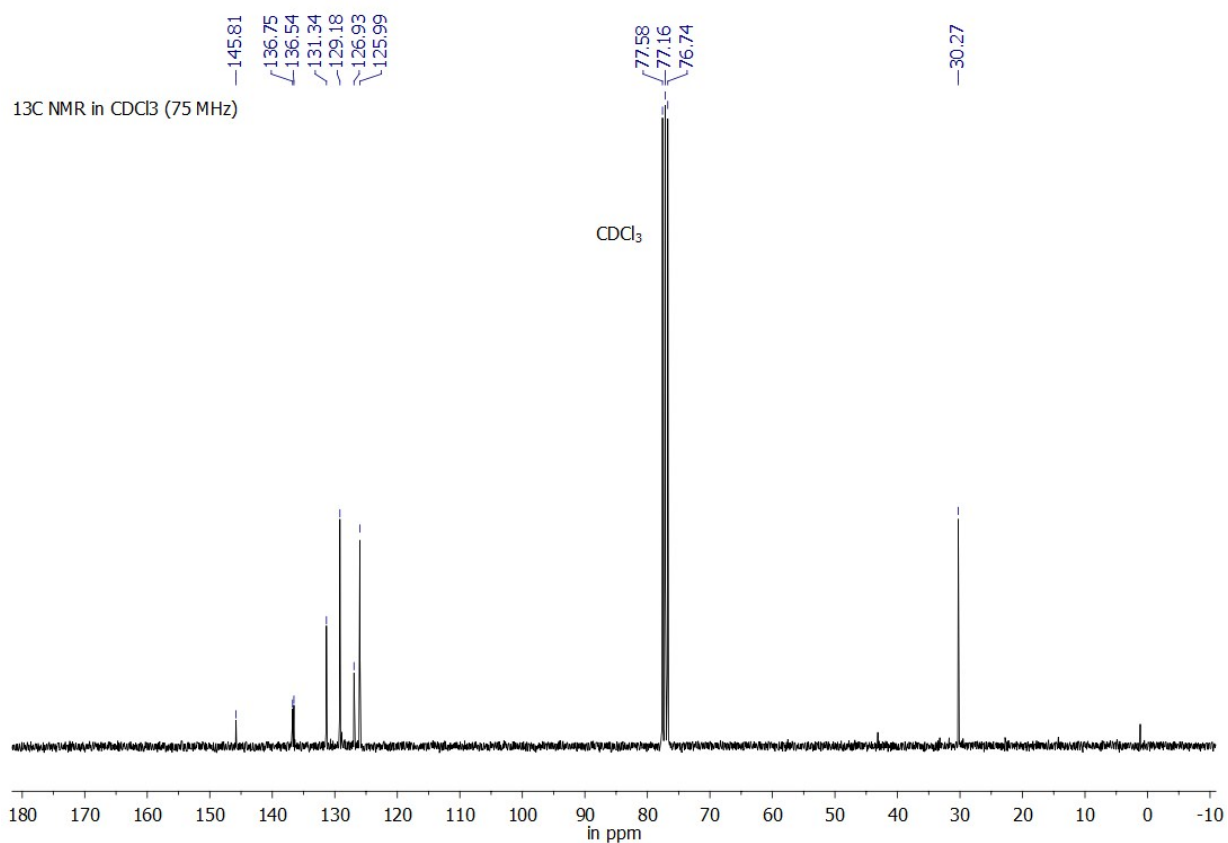


Figure S3.2: ¹³C NMR spectrum of **1** in CDCl₃.

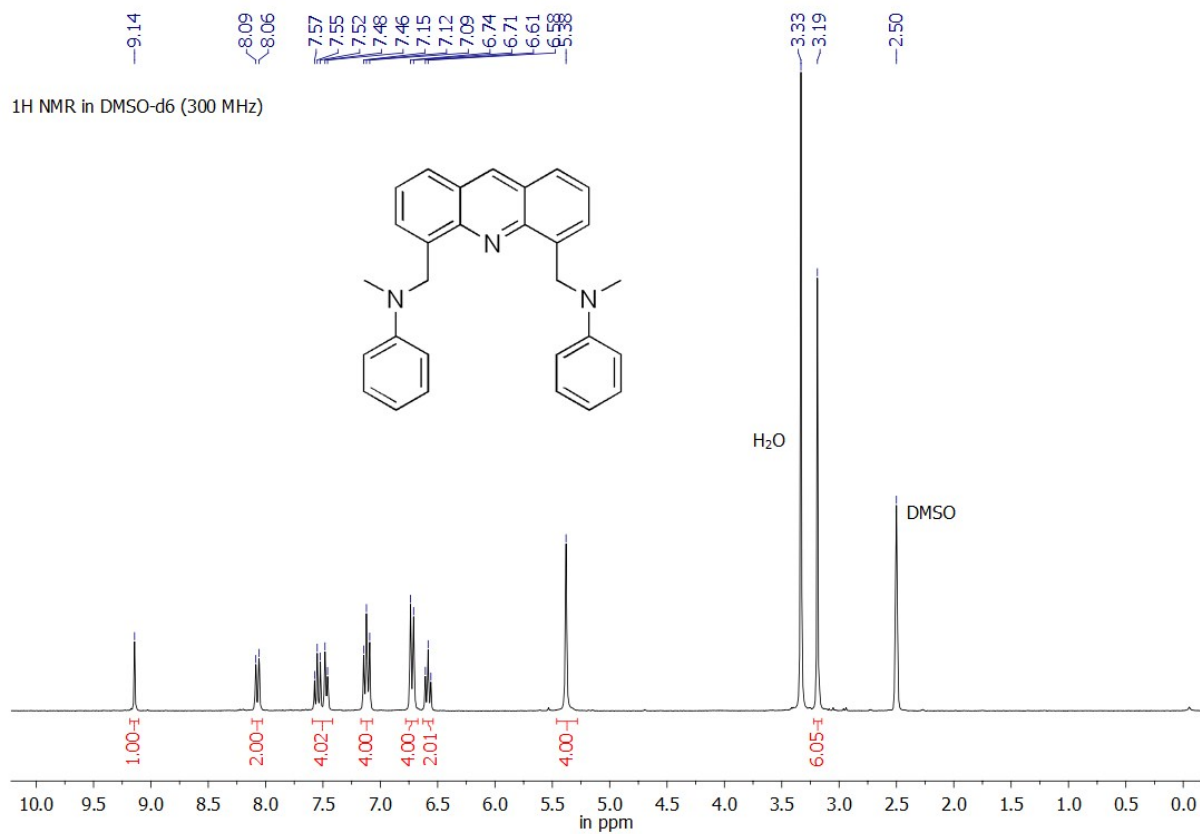


Figure S3.3: ¹H NMR spectrum of **2** in DMSO-d₆.

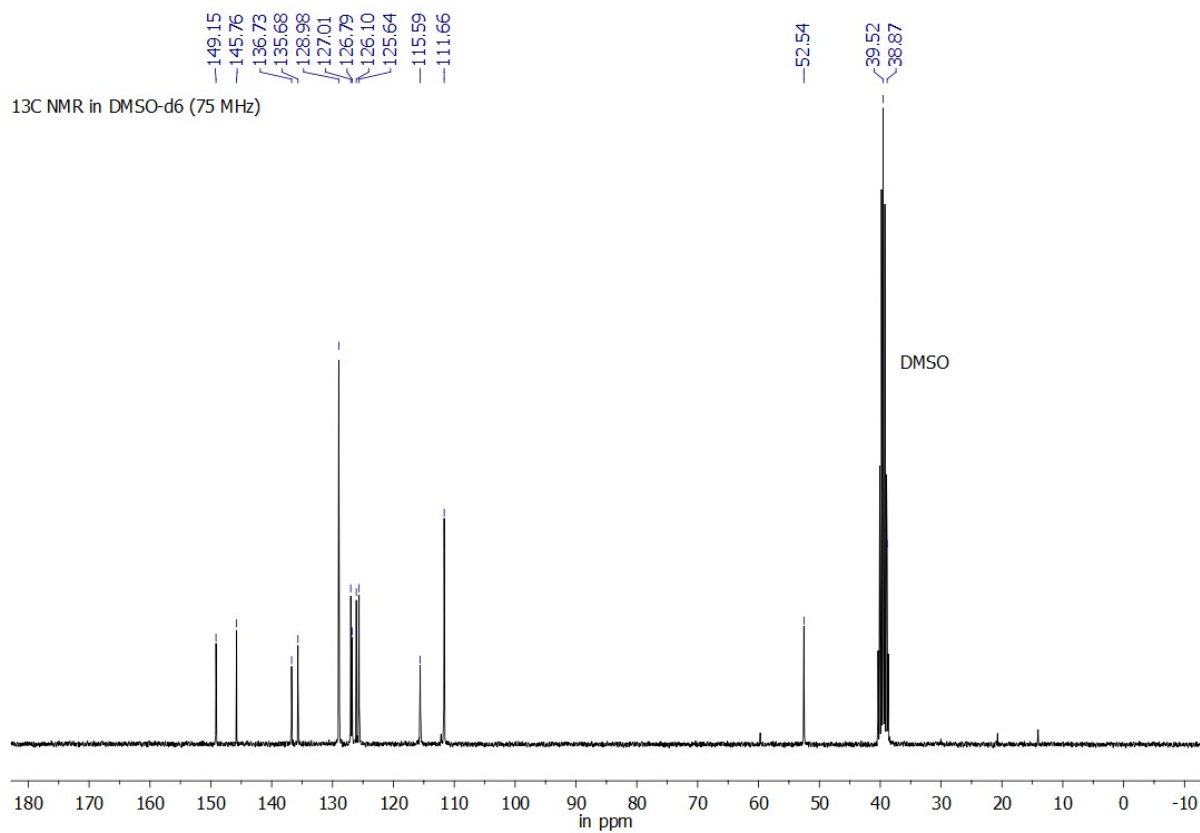


Figure S3.4: ¹³C NMR spectrum of **2** in DMSO-d₆.

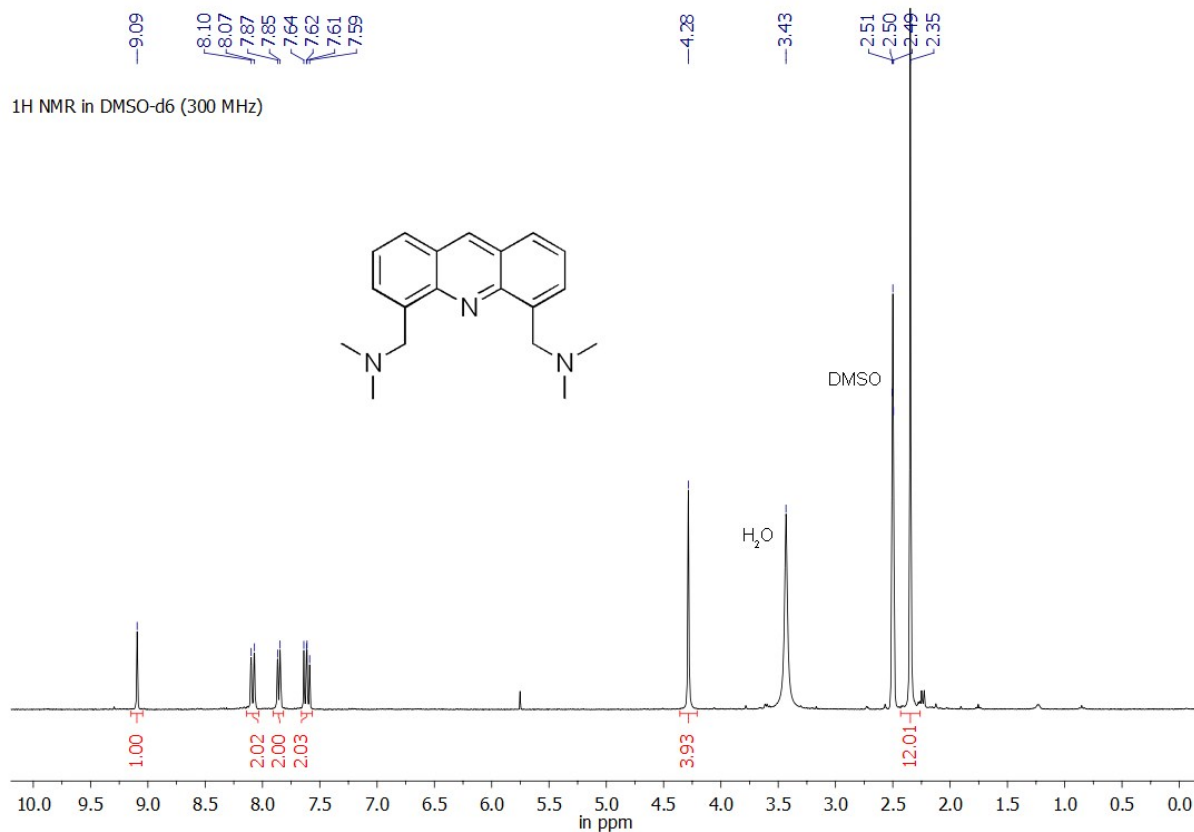


Figure S3.5: ¹H NMR spectrum of **3** in DMSO-d₆.

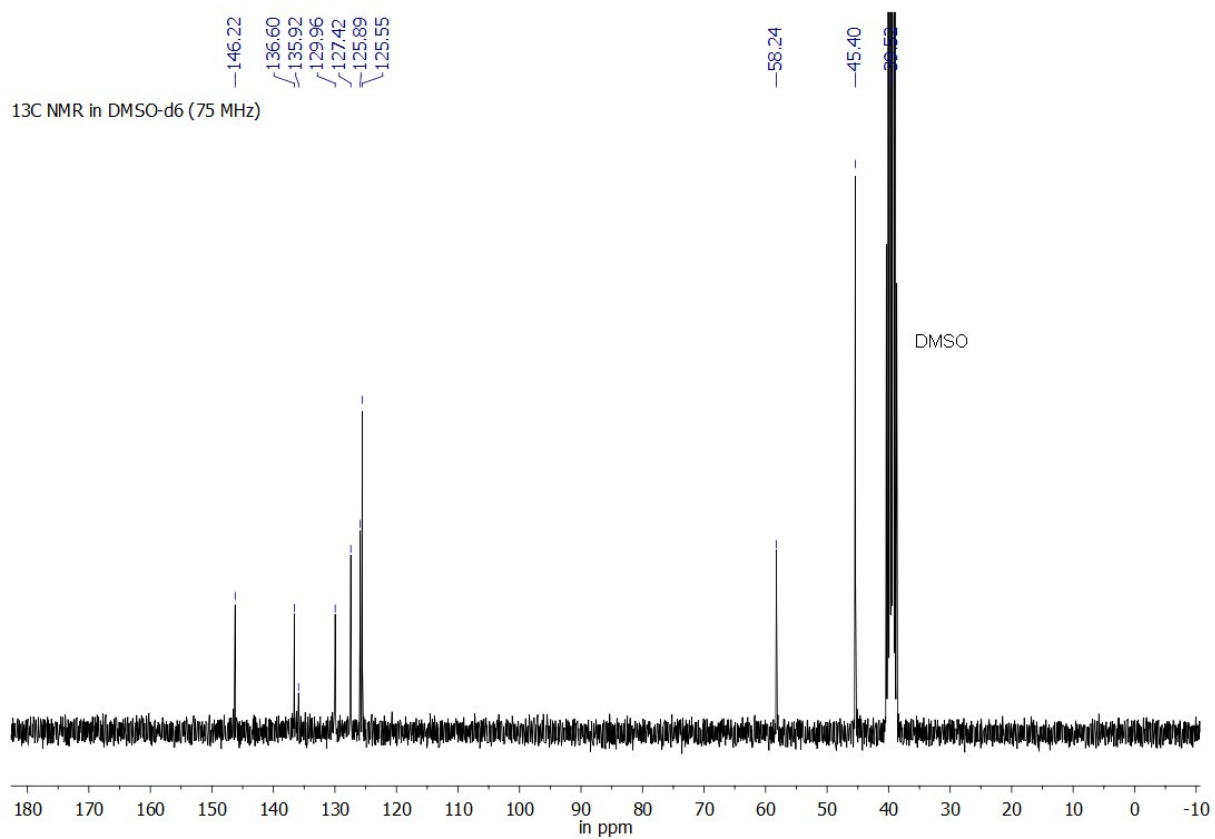


Figure S3.6: ¹³C NMR spectrum of **3** in DMSO-d₆.

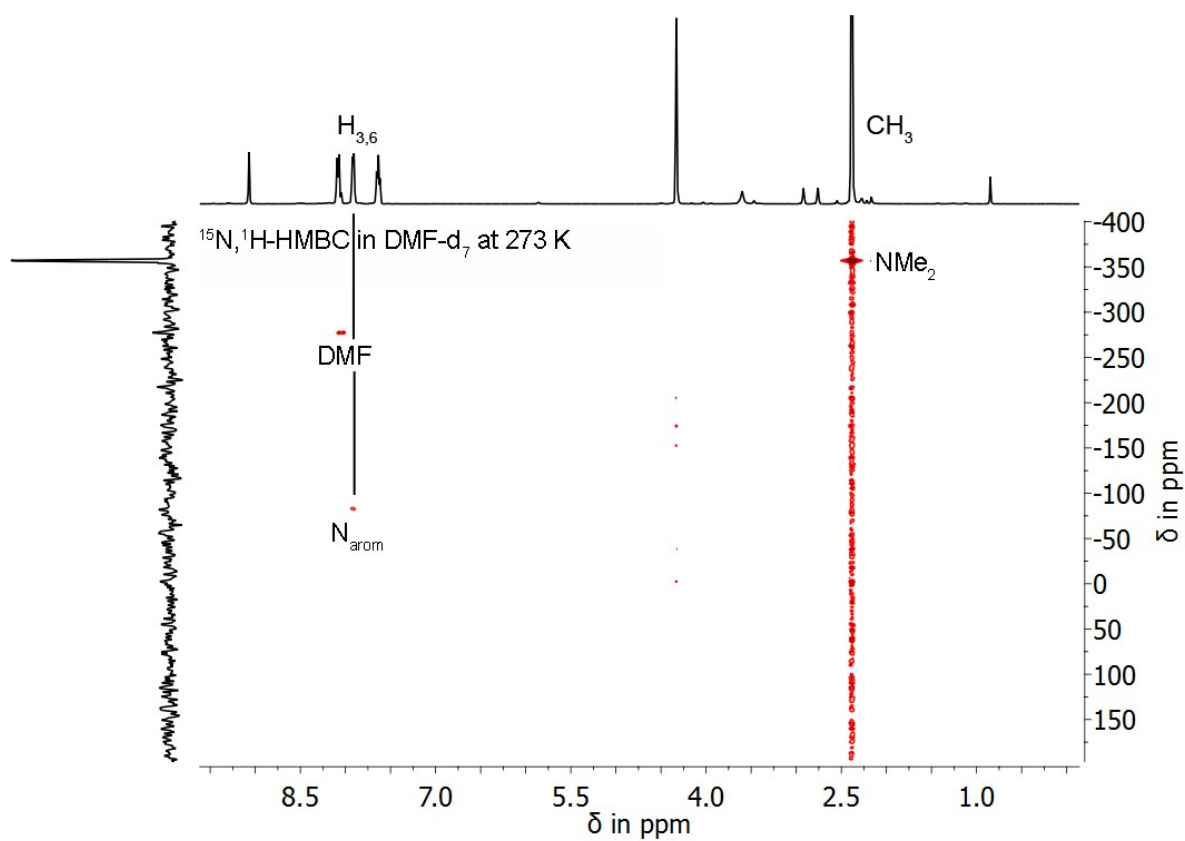


Figure S3.7: $^{15}\text{N}, ^1\text{H}$ -HMBC NMR spectrum of **3** in DMF-d_7 at 273 K.

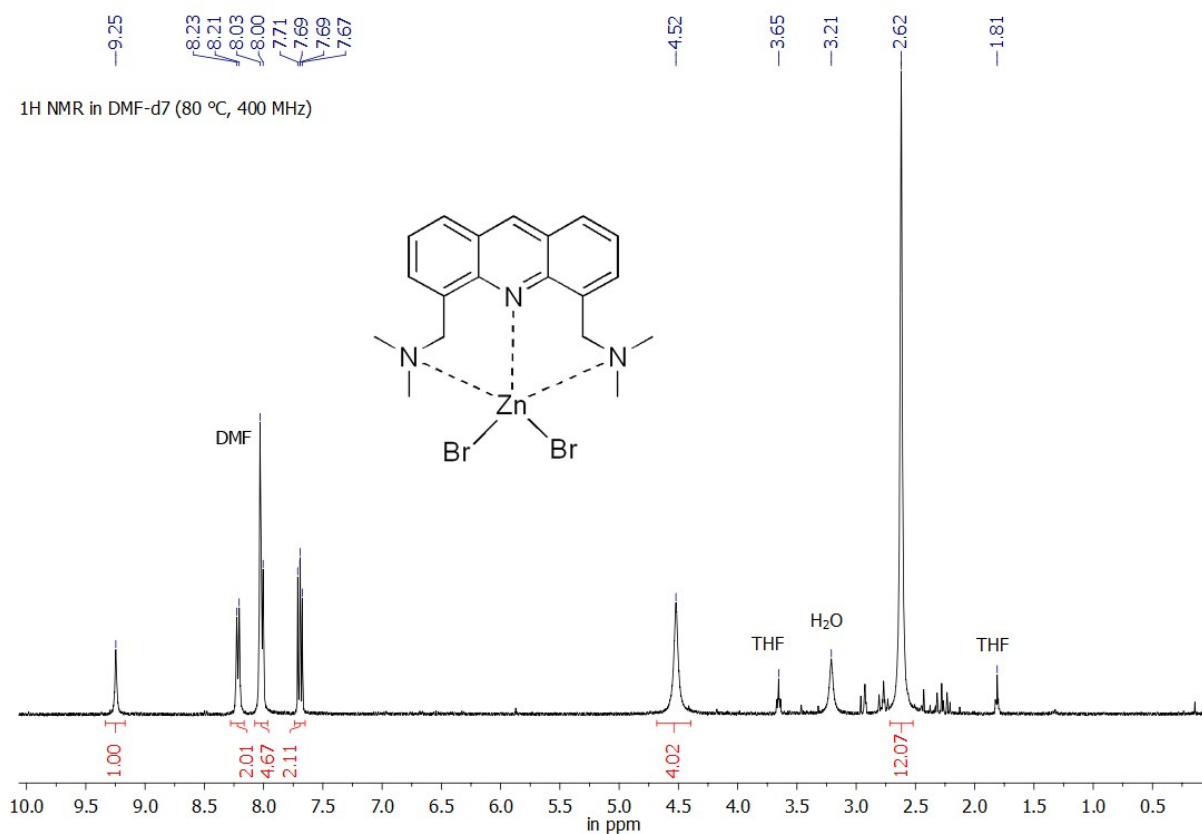


Figure S3.8: ¹H NMR spectrum of **4** in DMF-d₇ at 353 K.

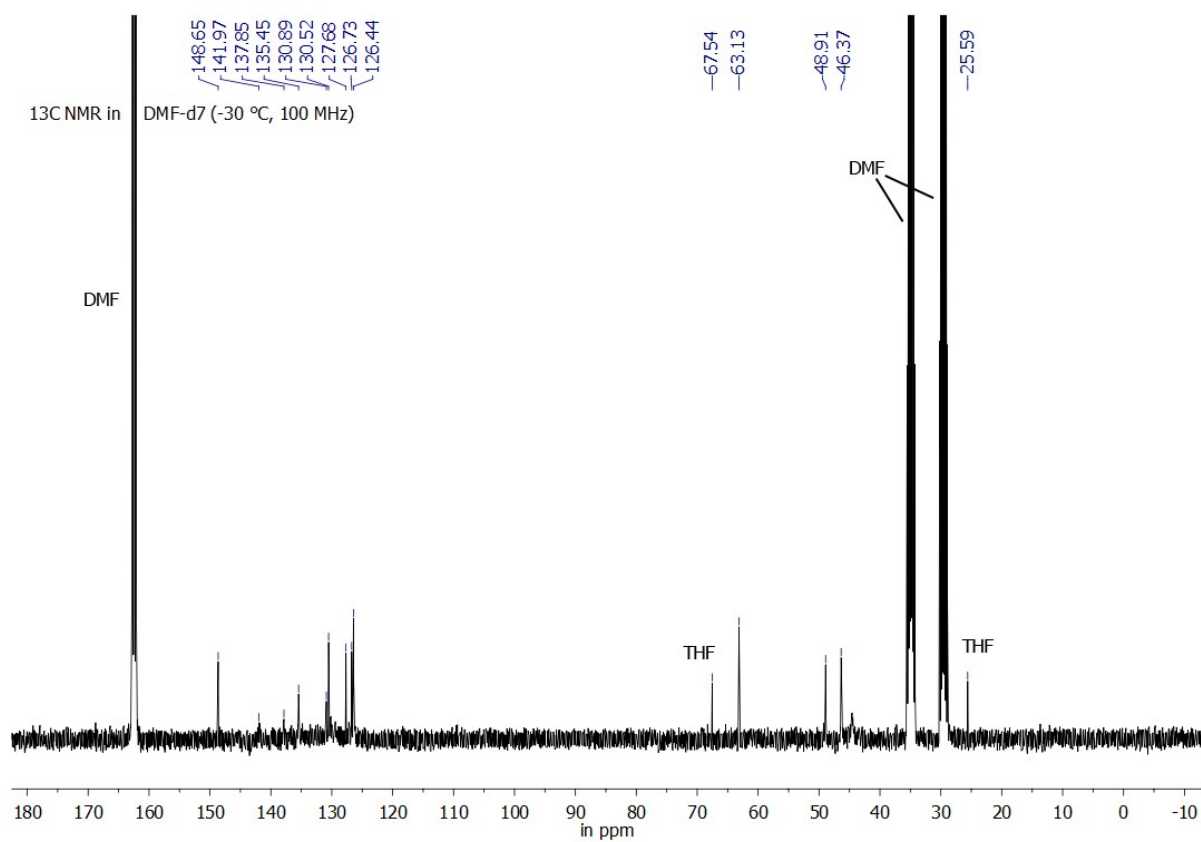


Figure S3.9: ¹³C NMR spectrum of **4** in DMF-d₇ at 243 K.

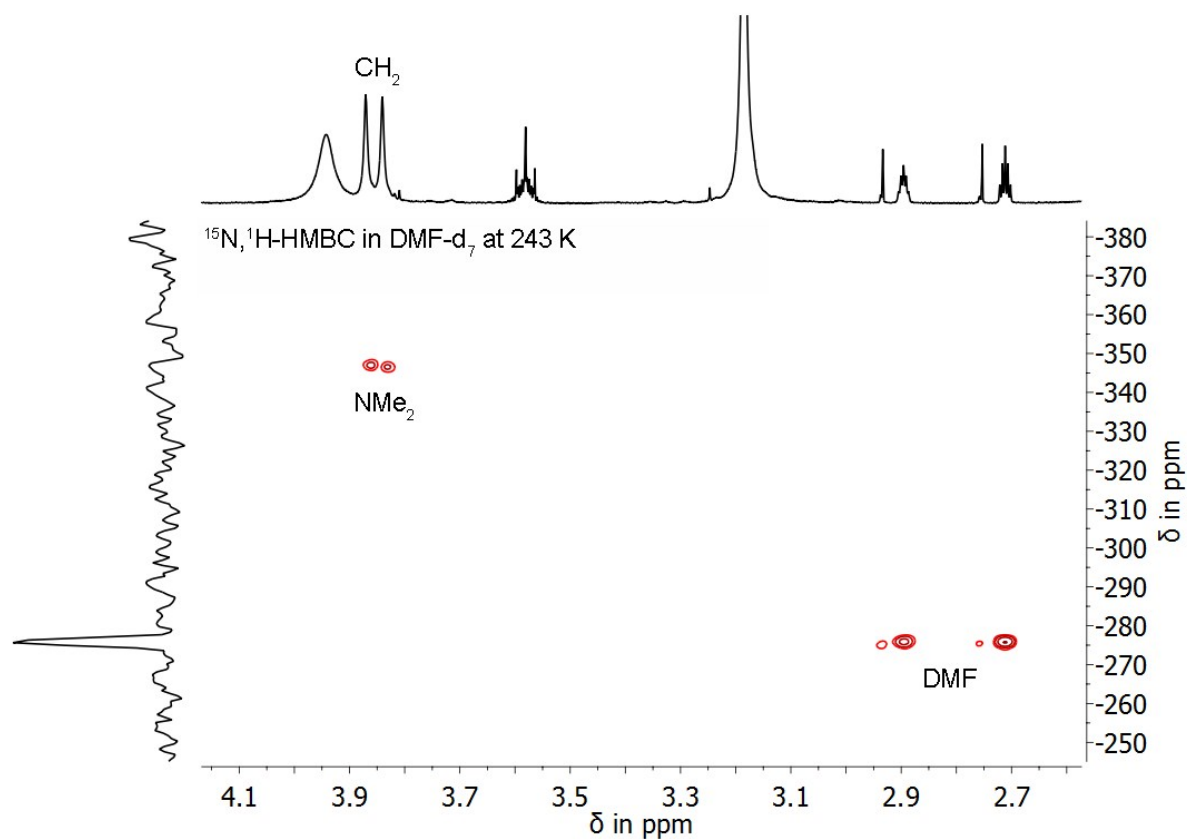


Figure S3.10: $^{15}\text{N}, ^1\text{H}$ -HMBC NMR spectrum of **4** in DMF-d_7 at 243 K.

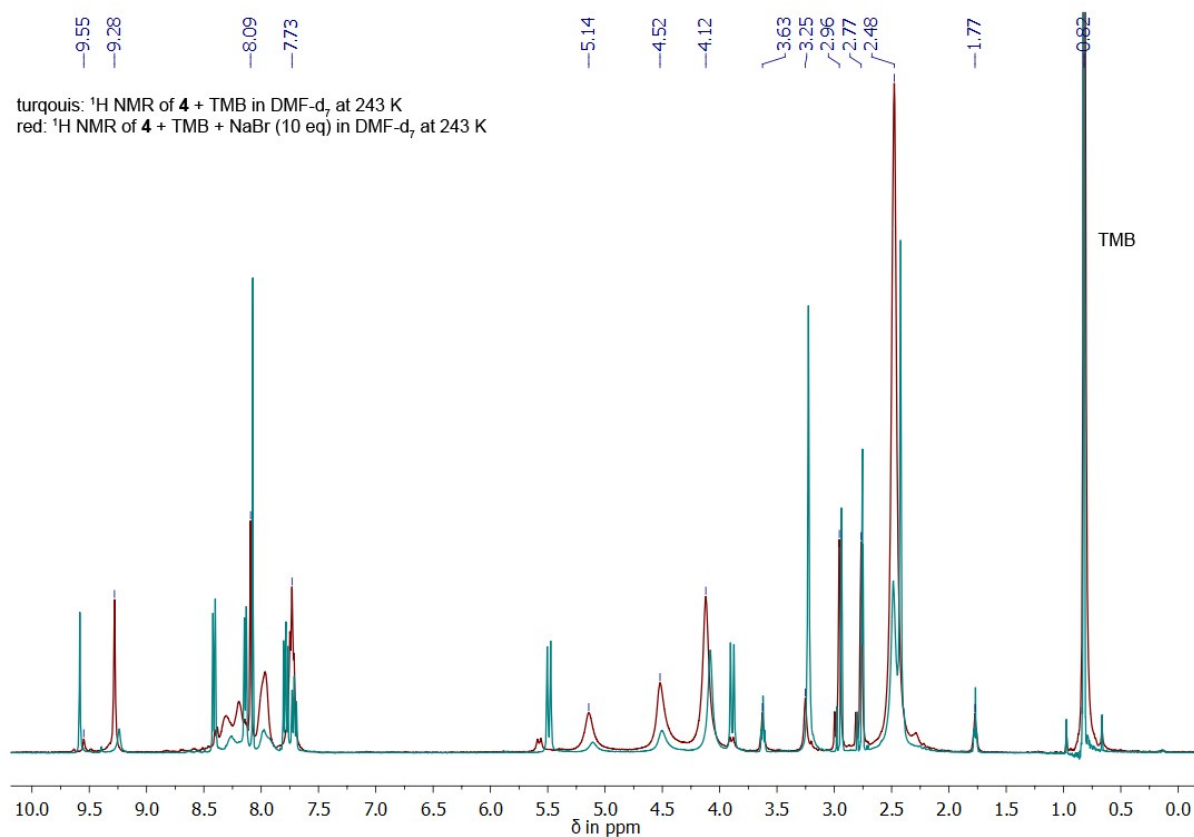


Figure S3.11: Superimposed ^1H NMR spectra of **4** without (turquoise) and with addition of 10 eq NaBr (red) in DMF-d_7 at 243 K. Tetramethylbutane (TMB) was added as internal reference for the subsequent ^1H DOSY NMR spectrum.

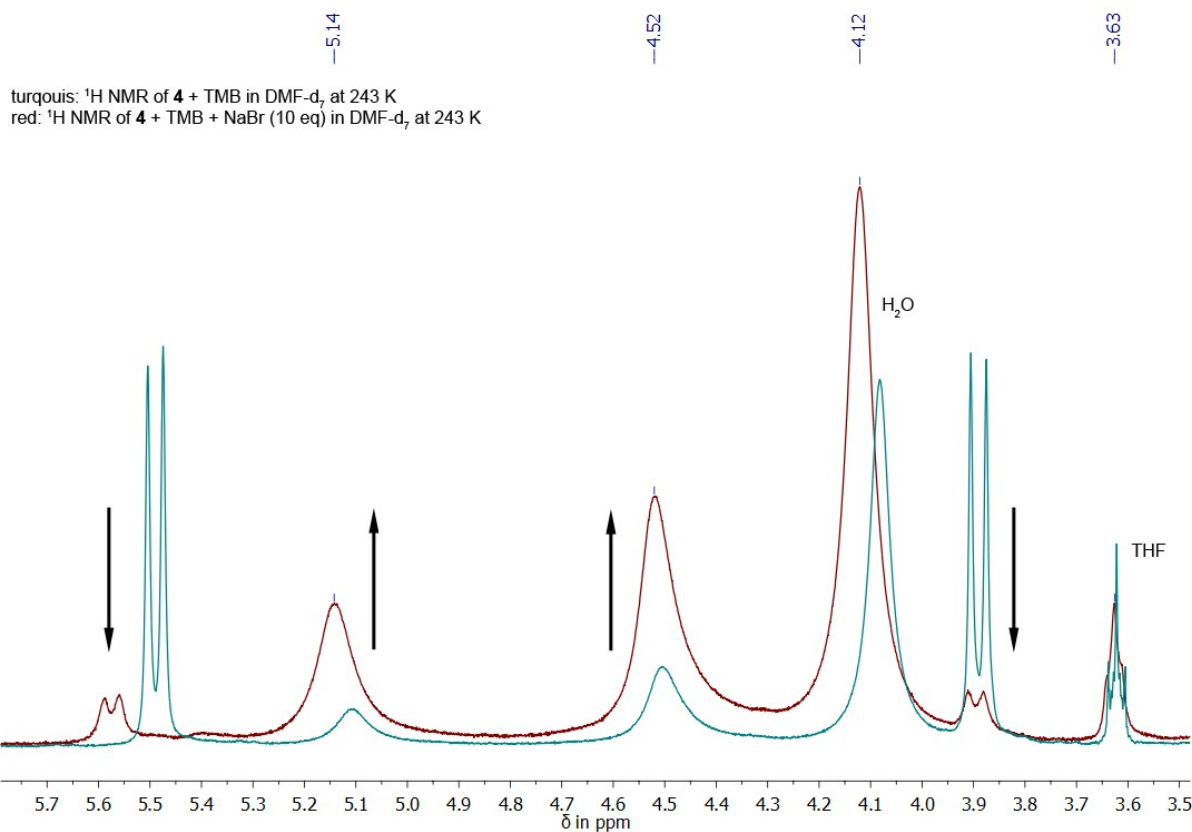


Figure S3.12: Extract of the superimposed ^1H NMR spectra of **4** without (turquoise) and with addition of 10 eq NaBr (red) in DMF-d_7 at 243 K. After the addition of the salt, the signal intensity of the diastereotopic methylene protons (CH_2) decreases, while two different signals at 5.14 and 4.52 ppm rise.

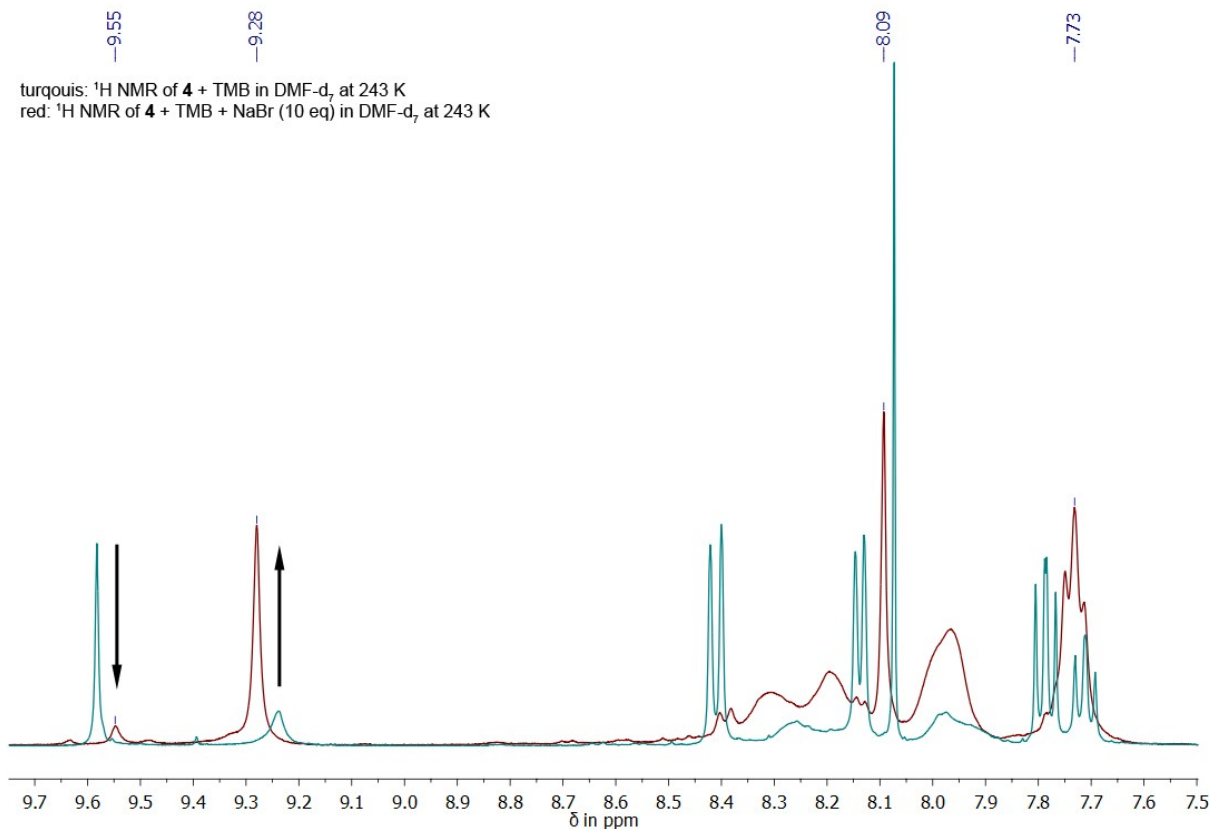


Figure S3.13: Extract of the superimposed ^1H NMR spectra of **4** without (turquoise) and with addition of 10 eq NaBr (red) in DMF-d_7 at 243 K. The signal intensities of the different species are nearly completely reversed.

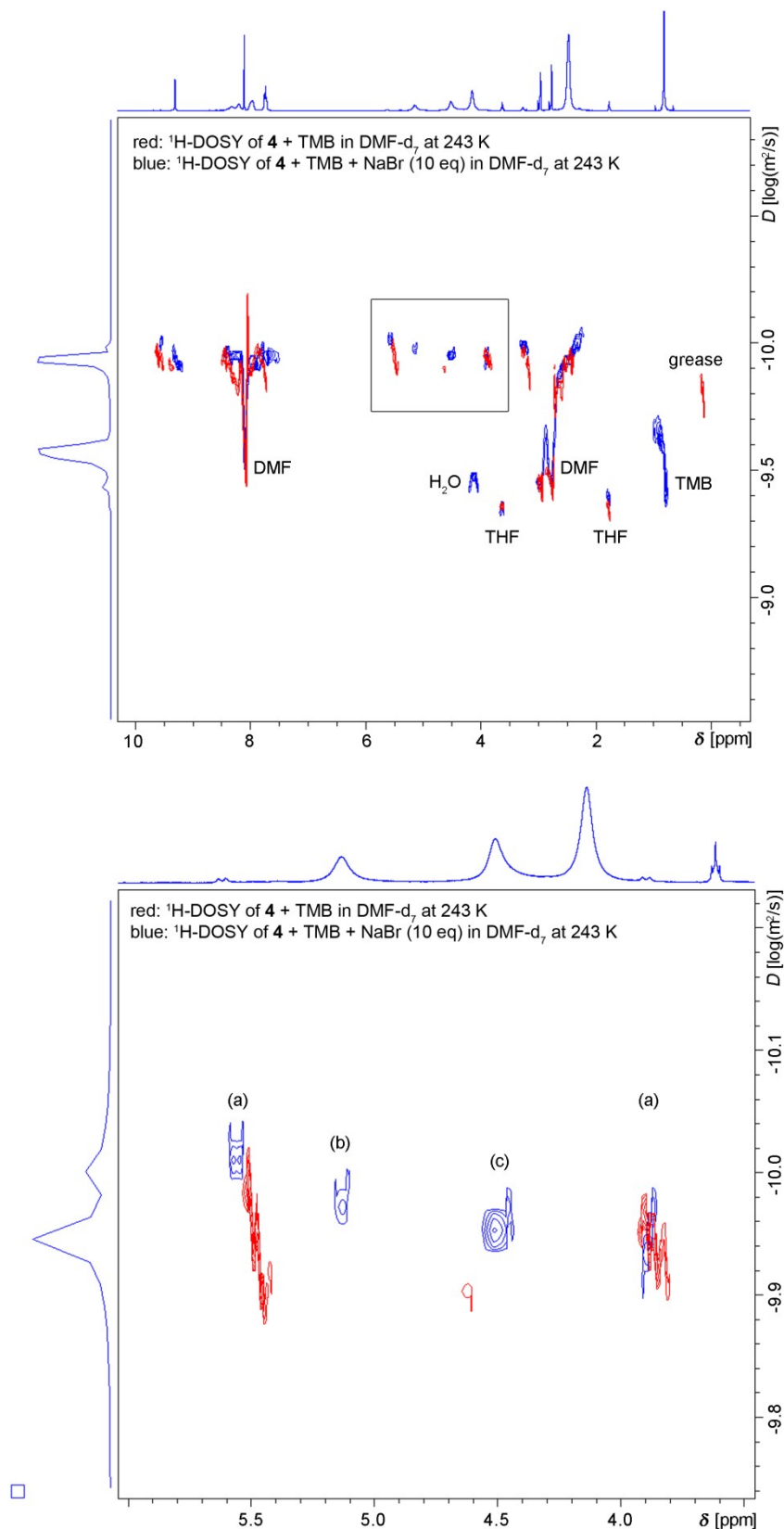


Figure S3.14: ^1H -DOSY NMR spectra of **4** without (red) and with addition of 10 eq NaBr (blue) in DMF- d_7 at 243 K (top: full spectrum; bottom: detail of the spectrum showing the signals of the CH₂ groups). Three different species can be observed after addition of NaBr which can be differentiated by their diffusion coefficient. We suggest the following aggregates: a) $[(\text{dmf})_2\text{Zn}\{(\text{Me}_2\text{NCH}_2)_2\text{Acr}\}]^{2+} \rightarrow$ b) $[(\text{dmf})\text{ZnBr}\{(\text{Me}_2\text{NCH}_2)_2\text{Acr}\}]^+ \rightarrow$ c) $[\text{ZnBr}_2\{(\text{Me}_2\text{NCH}_2)_2\text{Acr}\}]$. The diffusion coefficients of the signals decrease slightly from a) to c) which can be explained by the smaller size of a bromine atom compared to a DMF molecule: van-der-Waals volume of bromine: 2.74^{-29} m^3 / DMF: 1.31^{-28} m^3 .¹⁵

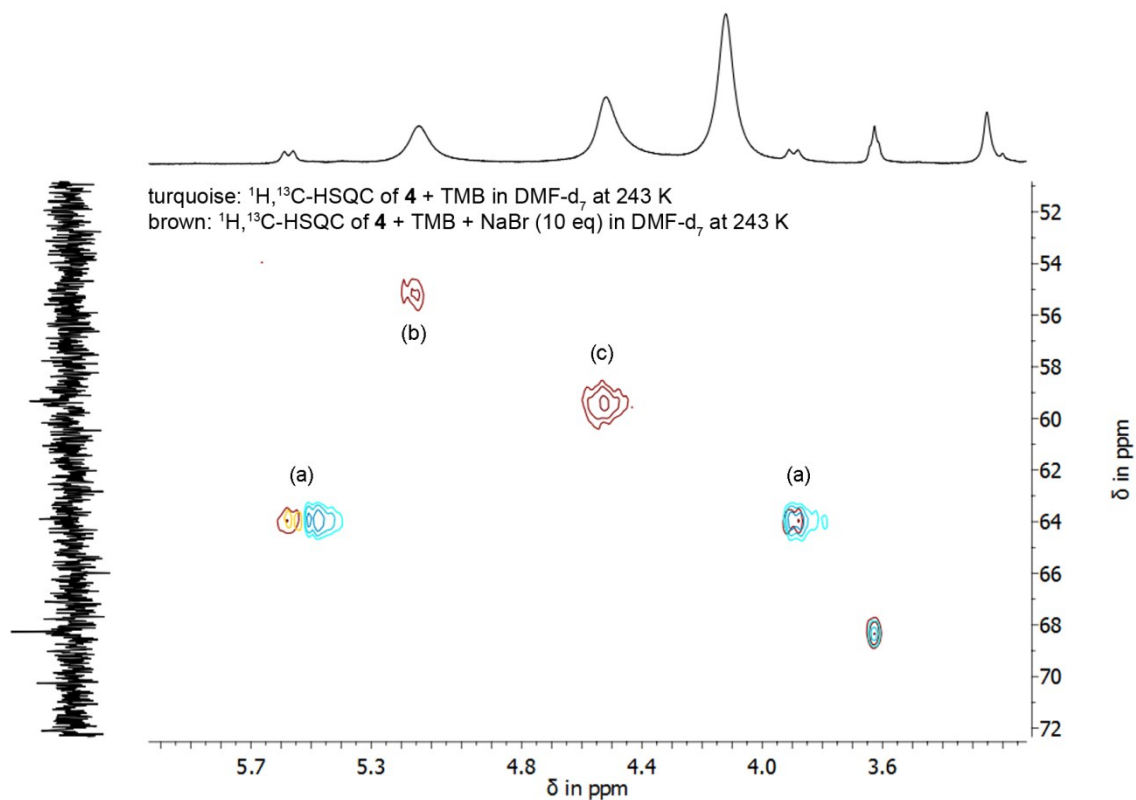


Figure S3.15: Superimposed $^1\text{H}, ^{13}\text{C}$ -HSQC NMR spectra of **4** without (turquoise) and with addition of 10 eq NaBr (brown) in DMF-d_7 at 243 K; a) $[(\text{dmf})_2\text{Zn}\{(\text{Me}_2\text{NCH}_2)_2\text{Acr}\}]^{2+}$; b) $[(\text{dmf})\text{ZnBr}\{(\text{Me}_2\text{NCH}_2)_2\text{Acr}\}]^+$; c) $[\text{ZnBr}_2\{(\text{Me}_2\text{NCH}_2)_2\text{Acr}\}]$. This spectrum is in line with the theory of generating different species by adding NaBr to the NMR sample. The protons of (a), (b), and (c) couple to different carbon atoms and do not belong to one compound.

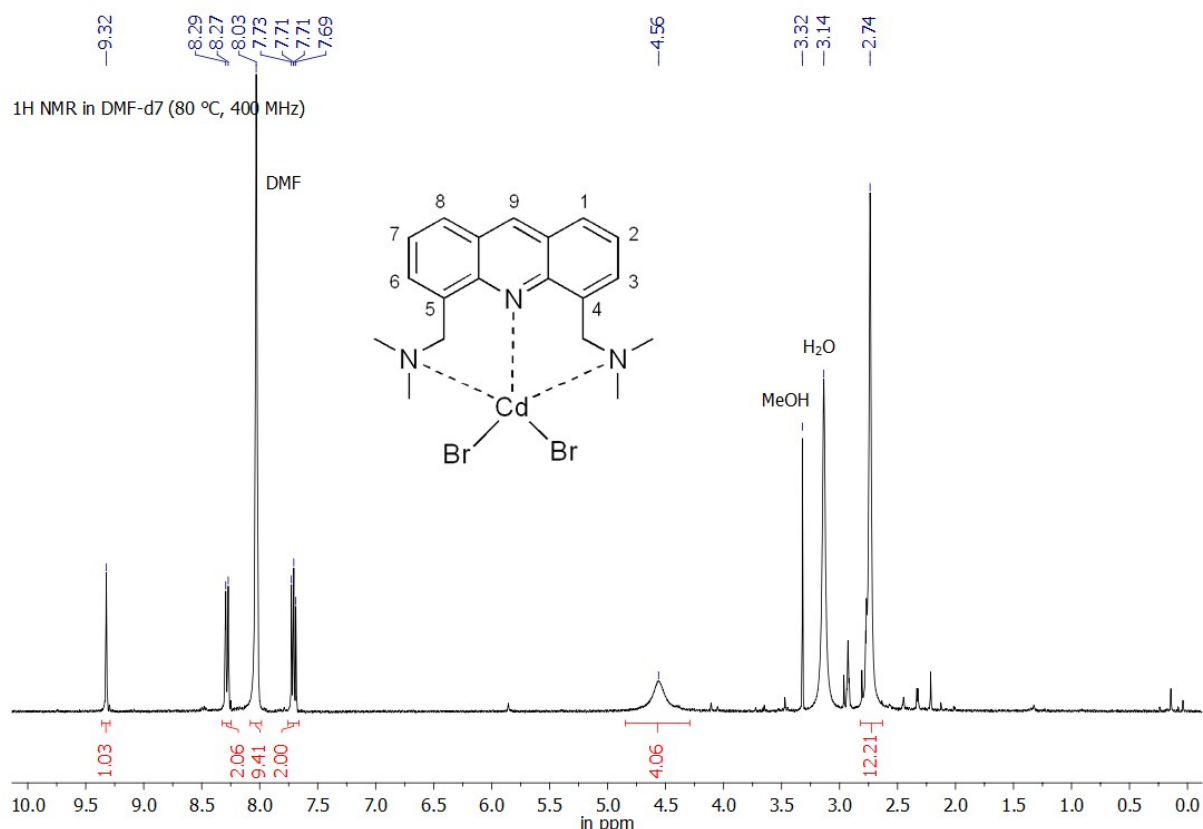


Figure S3.16: ¹H NMR spectrum of **5** in DMF-d₇ at 353 K. The signal of the protons H3/H6 is covered by the signal of the solvent DMF at 8.03 ppm.

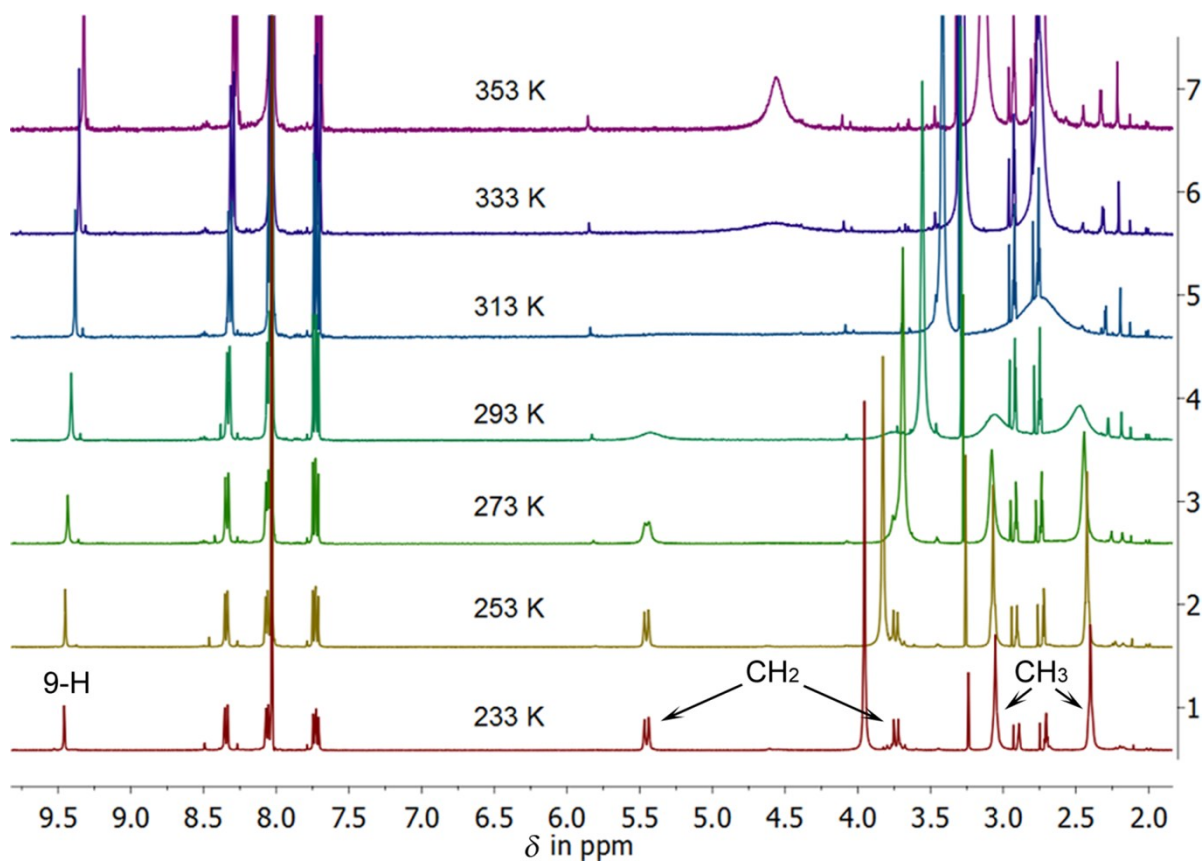


Figure S3.17: Temperature-dependent ¹H NMR spectra of **5** in DMF-d₇.

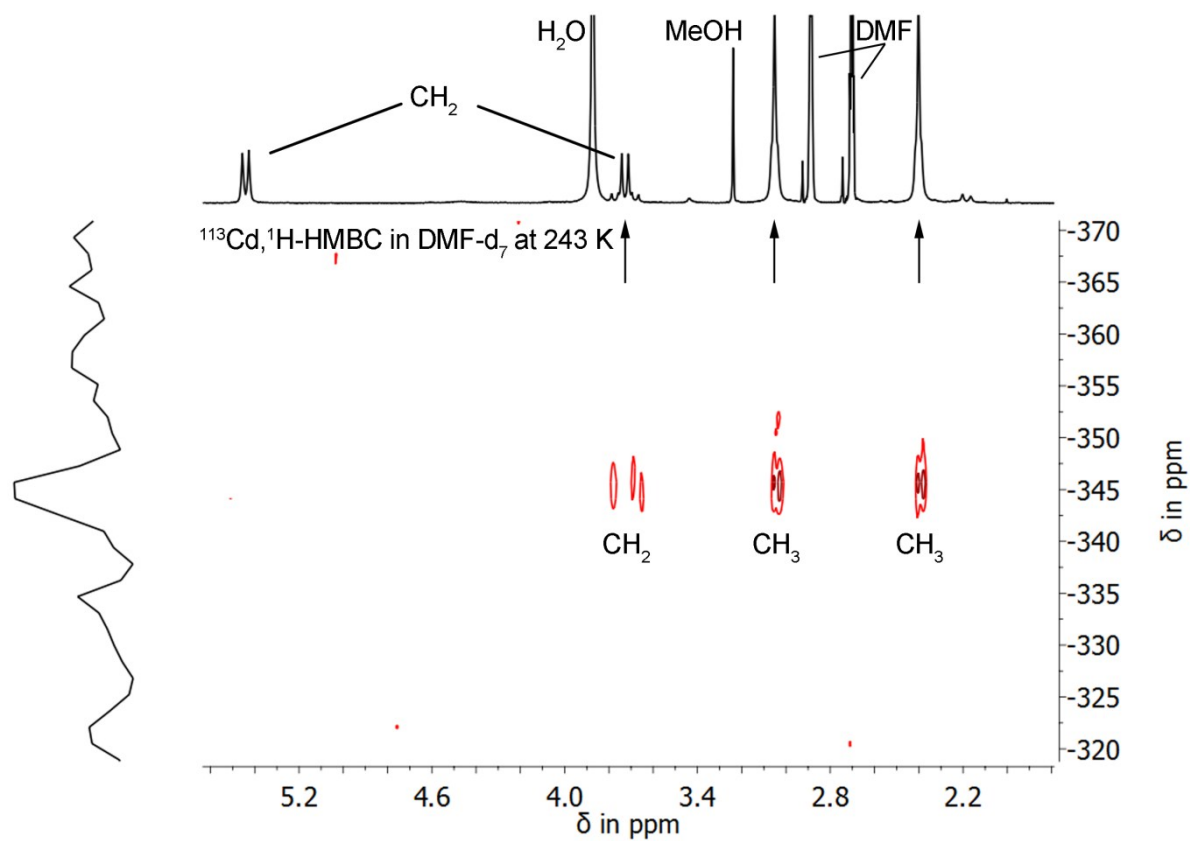


Figure S3.18: $^{113}\text{Cd}, ^1\text{H}$ -HMBC NMR spectrum of **5** in DMF-d_7 at 243 K. Only one proton of each CH_2 group is coupled to the ^{113}Cd nucleus ($\delta = -345$ ppm). The other coupling is likely not observed due to an unfavourable angle of the related atoms.¹⁶

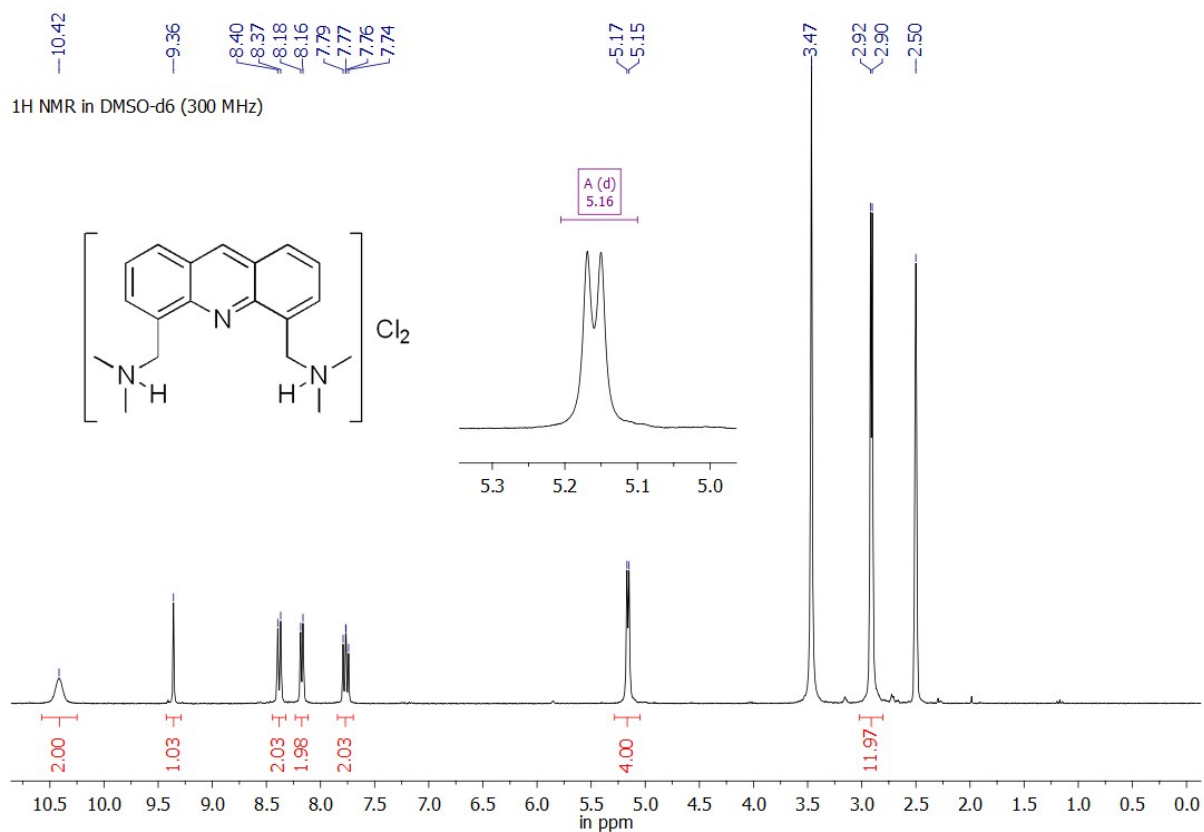


Figure S3.19: ¹H NMR spectrum of **6** in DMSO-d₆.

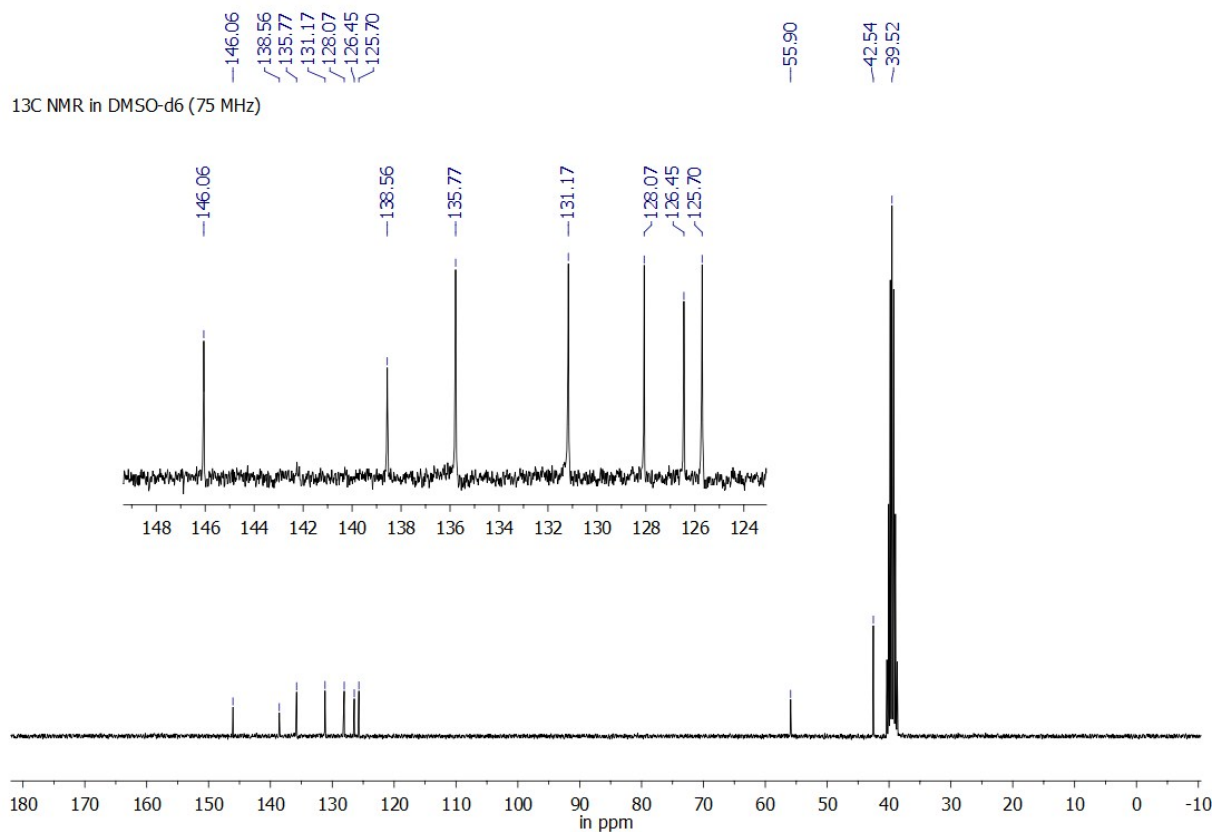


Figure S3.20: ¹³C NMR spectrum of **6** in DMSO-d₆.

4. UV/vis absorption spectra

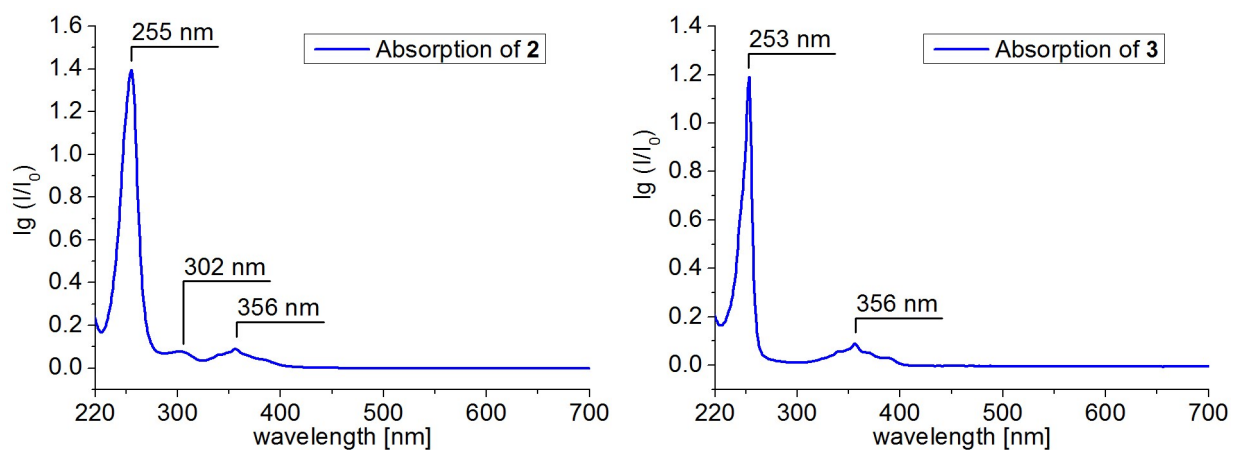


Figure S4.1: Absorption spectra of **2** (left) and **3** (right), measured in MeOH ($c = 1 \cdot 10^{-5}$ M).

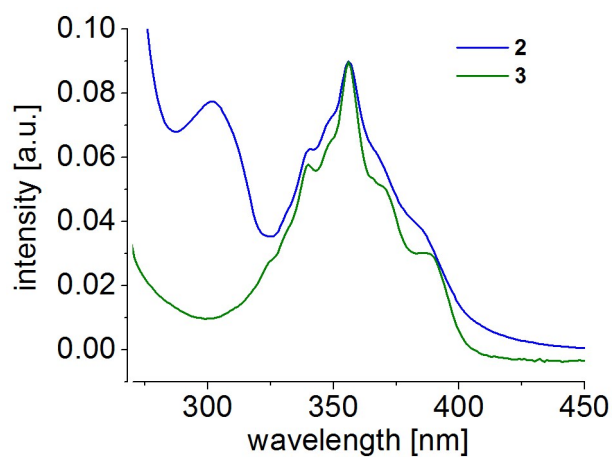


Figure S4.2: Comparison of the absorption spectra of **2** and **3** in the region around 350 nm, measured in MeOH ($c = 1 \cdot 10^{-5}$ M).

5. Fluorescence spectra

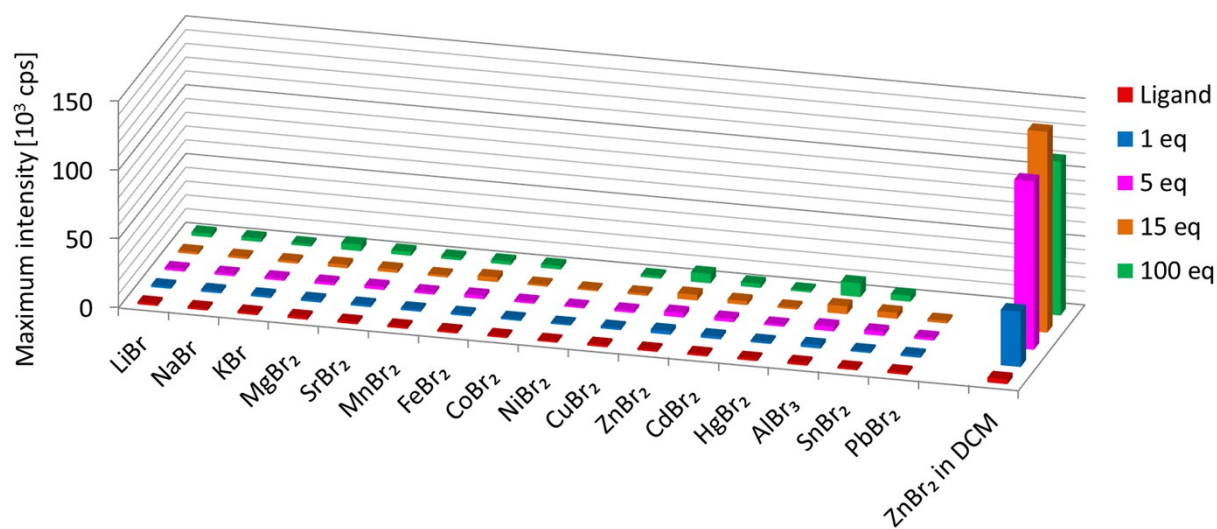


Figure S5.1: Metal ion screening with **2** in methanol as solvent. The maximum emission intensity is depicted at each metal ion addition. Only the measurement in the last column was done in DCM (the ligand as well as the ZnBr₂ were dissolved in DCM).

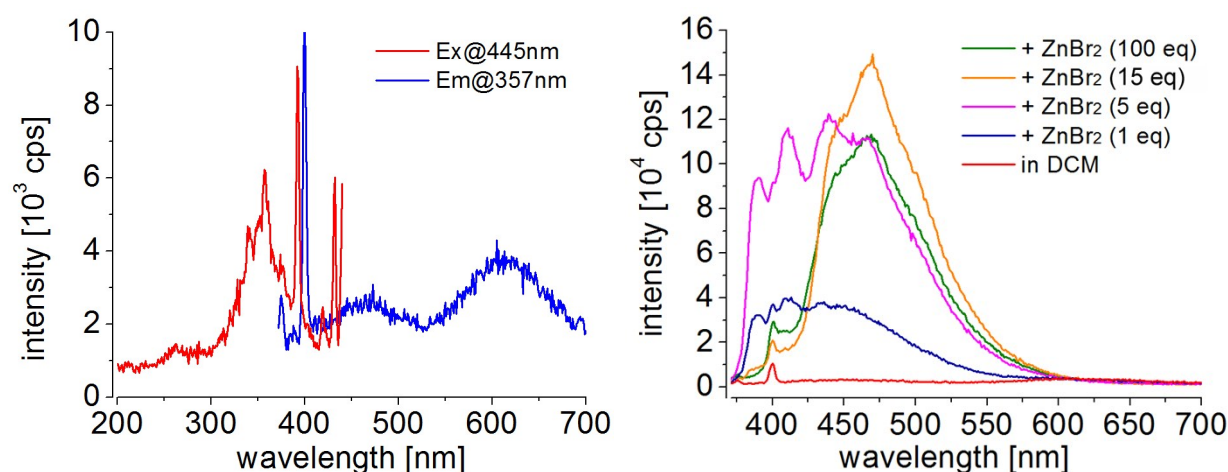


Figure S5.2: Left: Excitation (red, $\lambda_{\text{det}} = 445$ nm) and emission spectrum (blue, $\lambda_{\text{exc}} = 357$ nm) of **2** in DCM; right: emission spectra of **2** with addition of ZnBr₂ in DCM ($\lambda_{\text{exc}} = 357$ nm).

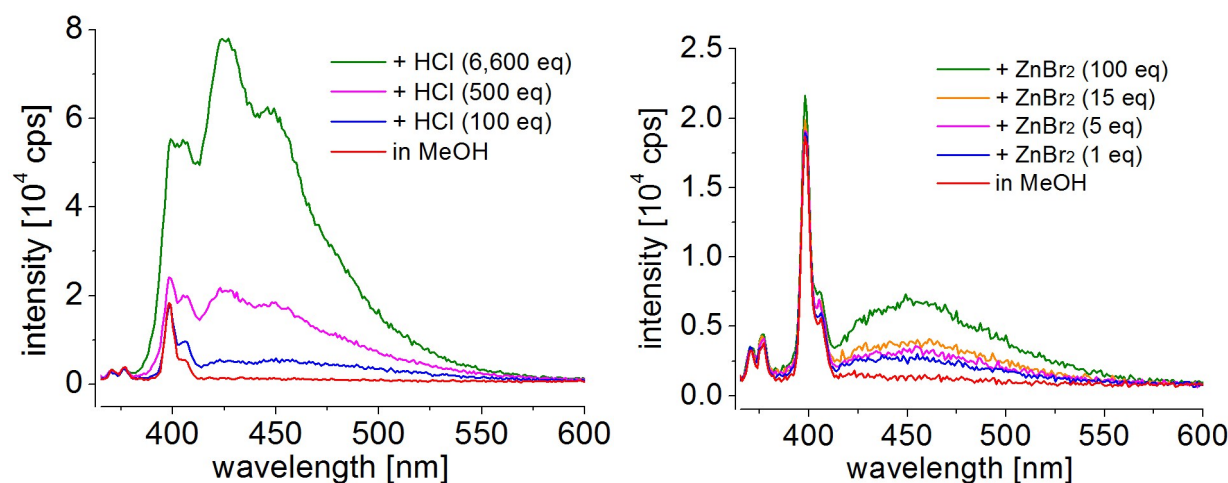


Figure S5.3: Emission spectra of **2** in methanol with addition of aqueous HCl (left) and with addition of ZnBr₂ in MeOH (right).

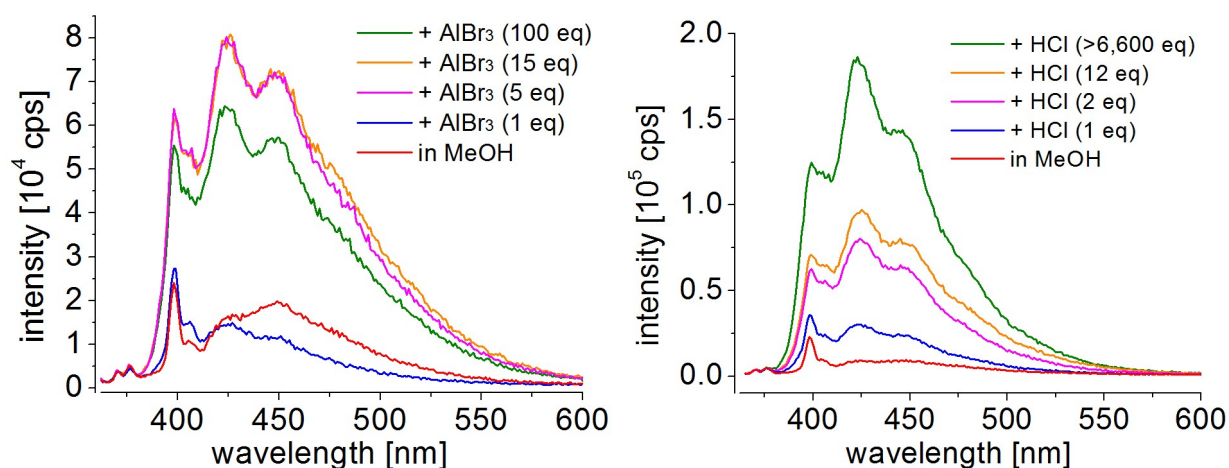


Figure S5.4: Comparison of the emission spectra of **3** after addition of AlBr₃ (left) and aqueous HCl (right). The maximum peak is in both cases at a wavelength of 425 nm.

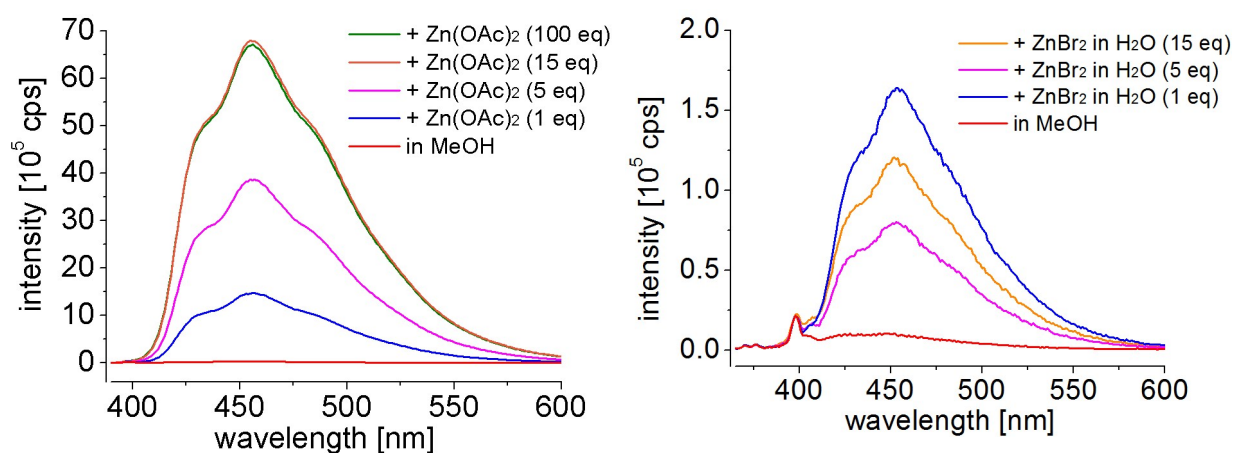


Figure S5.5: Emission spectra of **3** in methanol with various concentrations of Zn(OAc)₂ (left) and ZnBr₂ (right) which was dissolved before in purified water.

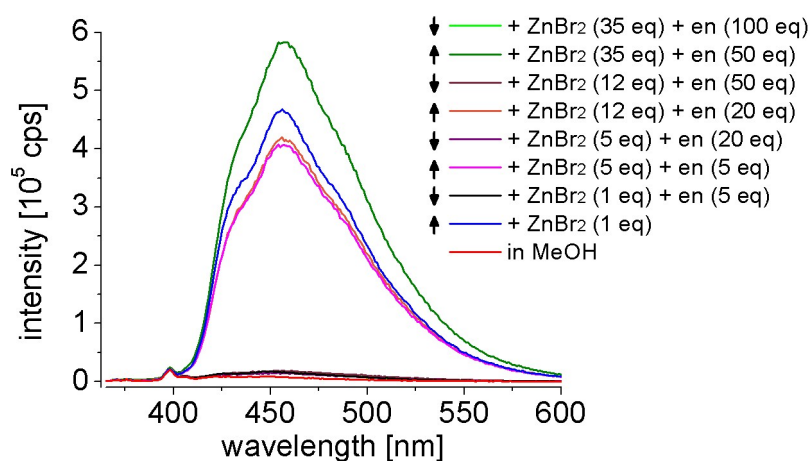


Figure S5.6: Reversibility of metal complexation of **3** with alternating addition of ZnBr₂ and ethylenediamine (en); all substances are dissolved in methanol.

6. Mass spectra

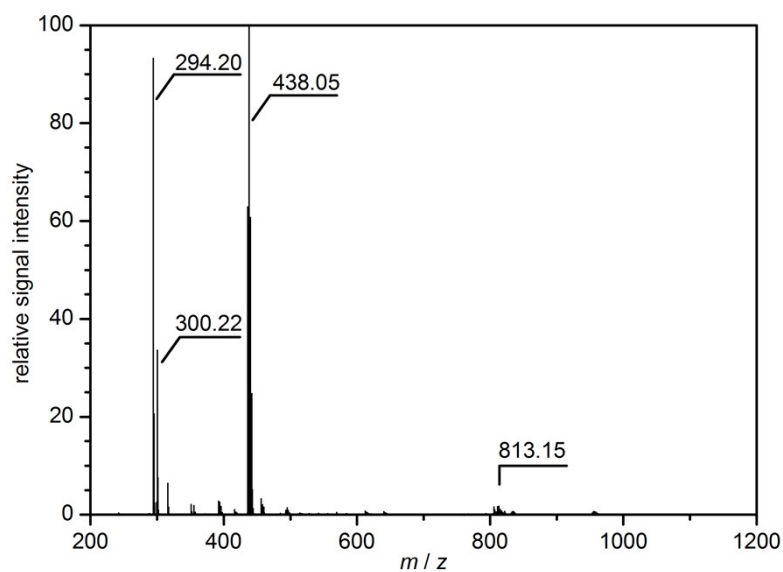


Figure S6.1: Positive-ion mode ESI-TOF mass spectrum of a solution of **4** in THF.

Table S6.1: Measured and theoretical m/z ratios of cations observed upon ESI-TOF-mass spectrometric analysis of **4** in THF.

Cation	m/z (measured)	m/z (theoretical)
$[(C_{19}H_{23}N_3)H]^+$	294.20	294.20
$[(C_{19}H_{23}N_3)Li]^+$	300.22	300.20
$[(C_{19}H_{23}N_3)ZnBr]^+$	438.05	438.03
$[(C_{19}H_{23}N_3)_2HZnBr_2]^+$	813.15	813.15

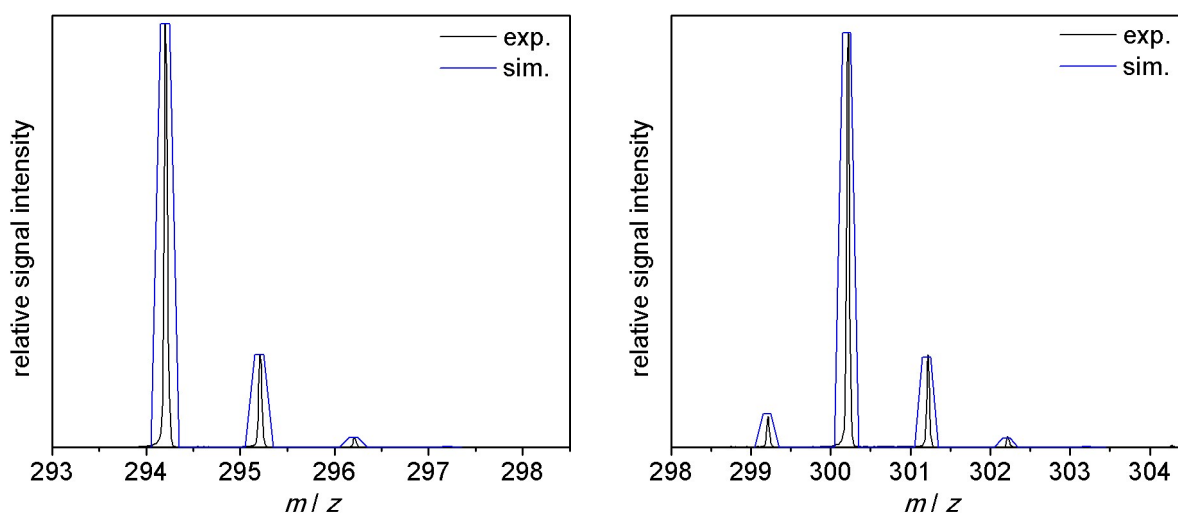


Figure S6.2: Parts of the mass spectrum of **4**, showing the experimental (black) and the simulated (blue) isotope pattern of $[(C_{19}H_{23}N_3)H]^+$ (left) and $[(C_{19}H_{23}N_3)Li]^+$ (right).

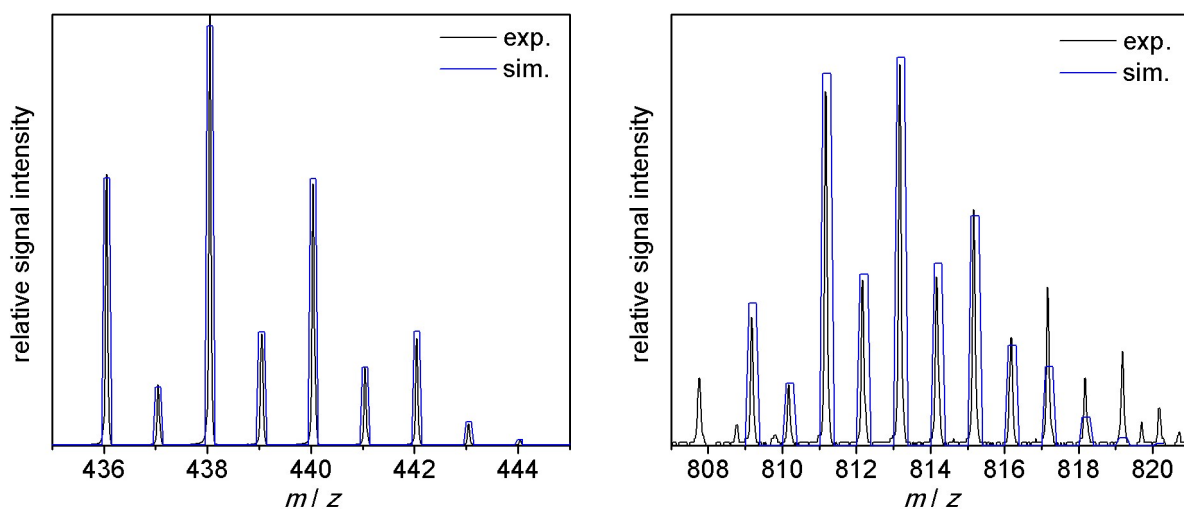


Figure S6.3: Parts of the mass spectrum of **4**, showing the experimental (black) and the simulated (blue) isotope pattern of $[(C_{19}H_{23}N_3)ZnBr]^+$ (left) and $[(C_{19}H_{23}N_3)_2HZnBr_2]^+$ (right).

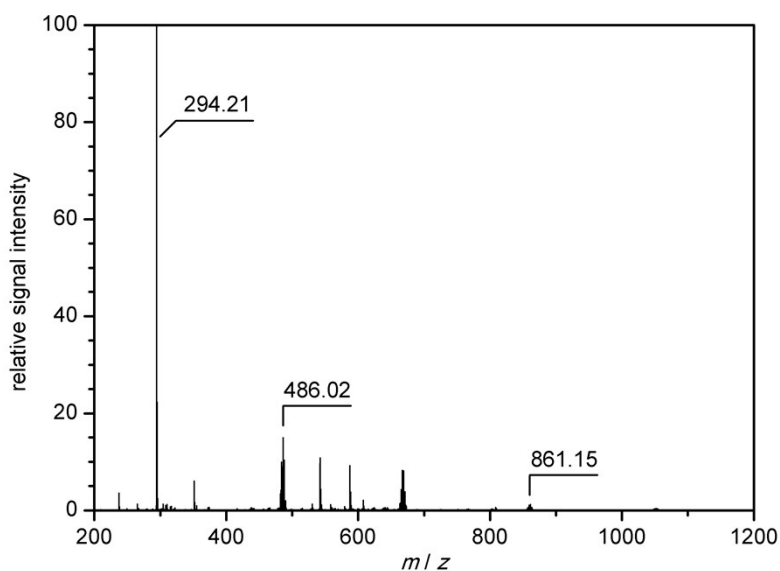


Figure S6.4: Positive-ion mode ESI-TOF mass spectrum of a solution of **5** in a THF/H₂O mixture.

Table S6.2: Measured and theoretical m/z ratios of cations observed upon ESI-TOF-mass spectrometric analysis of **5** in a THF/H₂O mixture.

Cation	m/z (measured)	m/z (theoretical)
$[(C_{19}H_{23}N_3)H]^+$	294.21	294.20
$[(C_{19}H_{23}N_3)CdBr]^+$	486.02	486.01
$[(C_{19}H_{23}N_3)_2HCdBr_2]^+$	861.15	861.12

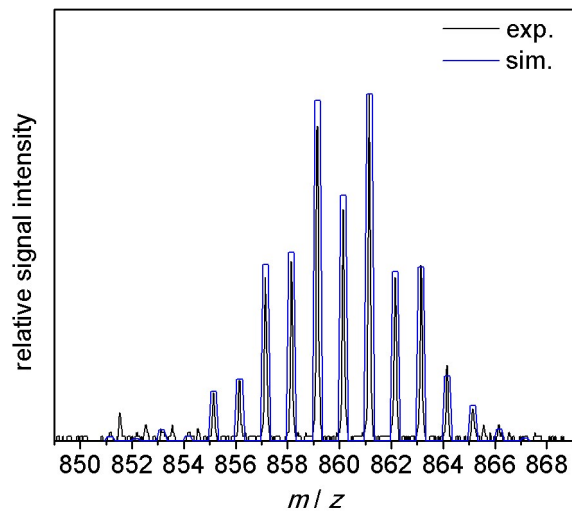
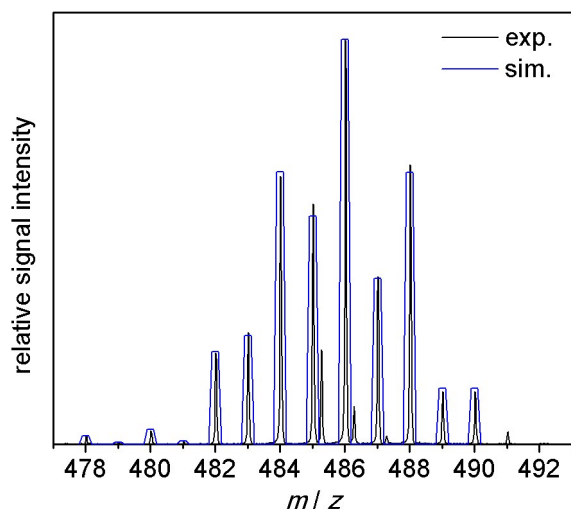


Figure S6.5: Parts of the mass spectrum of **5**, showing the experimental (black) and the simulated (blue) isotope pattern of $[(C_{19}H_{23}N_3)CdBr]^+$ (left) and $[(C_{19}H_{23}N_3)_2HCdBr_2]^+$ (right).

7. Crystallographic data

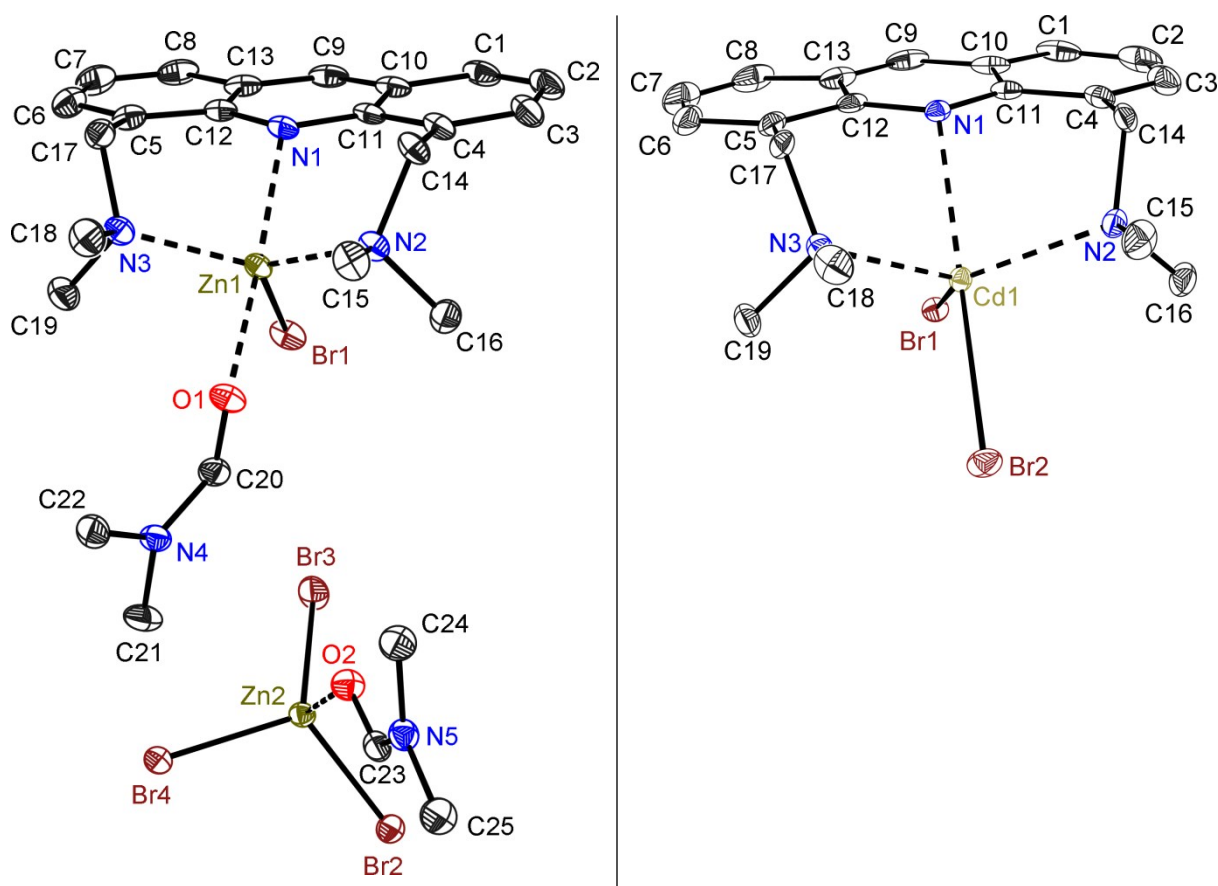


Figure S7.1: Solid state structures of $[(\text{dmf})\text{ZnBr}\{(\text{Me}_2\text{NCH}_2)_2\text{Acr}\}]^+[(\text{dmf})\text{ZnBr}_3]^-$ (**4a**, left) and $[\text{CdBr}_2\{(\text{Me}_2\text{NCH}_2)_2\text{Acr}\}]$ (**5**, right); All hydrogen atoms were omitted for clarity. Anisotropic displacement parameters are depicted at the 50% probability level.

Table S7.1: Selected bond lengths [pm] and angles [°].

	4a (Zn)	5 (Cd)		4a (Zn)	5 (Cd)
N1–M	230.39(16)	254.07(18)	N1–M–N2	90.05(6)	82.91(6)
N2–M	207.89(16)	232.31(19)	N1–M–N3	89.81(6)	82.81(6)
N3–M	209.09(17)	231.70(19)	N2–M–N3	128.68(6)	120.87(7)
Br1–M	239.83(4)	259.13(4)	N1–M–O1/Br2	175.31(6)	174.08(4)
O1/Br2–M	218.82(14)	266.16(4)	Br1–M–O1/Br2	94.40(4)	101.773(14)
O2–Zn2	203.61(15)	---	C14–N2–C15	107.02(15)	107.91(18)
Br2–Zn2	239.07(5)	---	C14–N2–C16	109.64(15)	110.15(19)
Br3–Zn2	236.74(5)	---	C15–N2–C16	108.34(16)	108.91(18)
Br4–Zn2	239.39(5)	---	C17–N3–C18	106.44(16)	107.69(18)
			C17–N3–C19	108.94(16)	110.03(19)
			C18–N3–C19	108.59(16)	109.33(18)
			C3–C4–C14–N2	–114.8(2)	–105.3(3)
			C6–C5–C17–N3	112.7(2)	105.9(3)

Table S7.2: Crystallographic data for compound **4a** and **5**.

Parameters	4a	5
CCDC no.	1061423	1061424
Empirical formula	C ₂₅ H ₃₇ Br ₄ N ₅ O ₂ Zn ₂	C ₁₉ H ₂₃ Br ₂ CdN ₃
Formula weight	889.97 g/mol	565.62 g/mol
Temperature	100(2) K	100(2) K
Wavelength	0.71073 Å	0.56086 Å
Crystal system	Monoclinic	Orthorhombic
Space group	<i>P</i> 2 ₁ / <i>c</i>	<i>P</i> 2 ₁ 2 ₁ 2 ₁
Unit cell dimensions	<i>a</i> = 20.985(3) Å; α = 90° <i>b</i> = 9.749(2) Å; β = 111.33(2)° <i>c</i> = 16.858(2) Å; γ = 90°	<i>a</i> = 11.135(2) Å; α = 90° <i>b</i> = 13.332(2) Å; β = 90° <i>c</i> = 13.562(3) Å; γ = 90°
Volume	3.2126(10) nm ³	2.0133(6) nm ³
<i>Z</i>	4	4
Density (calculated)	1.840 Mg/m ³	1.866 Mg/m ³
Absorption coefficient	6.499 mm ⁻¹	2.706 mm ⁻¹
<i>F</i> (000)	1752	1104
Crystal size	0.212 x 0.179 x 0.076 mm ³	0.225 x 0.222 x 0.185 mm ³
θ range for data collection	1.042 to 27.891°	1.690 to 21.684°
Index ranges	-27 ≤ <i>h</i> ≤ 27, -12 ≤ <i>k</i> ≤ 12, -22 ≤ <i>l</i> ≤ 22	-14 ≤ <i>h</i> ≤ 14, -17 ≤ <i>k</i> ≤ 17, -17 ≤ <i>l</i> ≤ 17
Reflections collected	194567	77405
Independent reflections	7674 [<i>R</i> _{int} = 0.0355]	4810 [<i>R</i> _{int} = 0.0392]
Completeness to θ_{\max}	99.9%	100.0%
Absorption correction	Semi-empirical from equivalents	Semi-empirical from equivalents
Max. and min. transmission	0.5631 and 0.3815	0.7447 and 0.6799
Refinement method	Full-matrix least-squares on <i>F</i> ²	Full-matrix least-squares on <i>F</i> ²
Data / restraints / parameters	7674 / 0 / 351	4810 / 0 / 231
Goodness-of-fit on <i>F</i> ²	1.046	1.014
Final <i>R</i> indices [<i>I</i> > 2σ(<i>I</i>)]	<i>R</i> ₁ = 0.0204, w <i>R</i> ₂ = 0.0528	<i>R</i> ₁ = 0.0121, w <i>R</i> ₂ = 0.0261
<i>R</i> indices (all data)	<i>R</i> ₁ = 0.0236, w <i>R</i> ₂ = 0.0542	<i>R</i> ₁ = 0.0129, w <i>R</i> ₂ = 0.0263
Absolute structure parameter	n/a	0.014(3)
Extinction coefficient	n/a	0.00180(13)
Largest diff. peak and hole	1.419 and -0.667 eÅ ⁻³	0.241 and -0.190 eÅ ⁻³

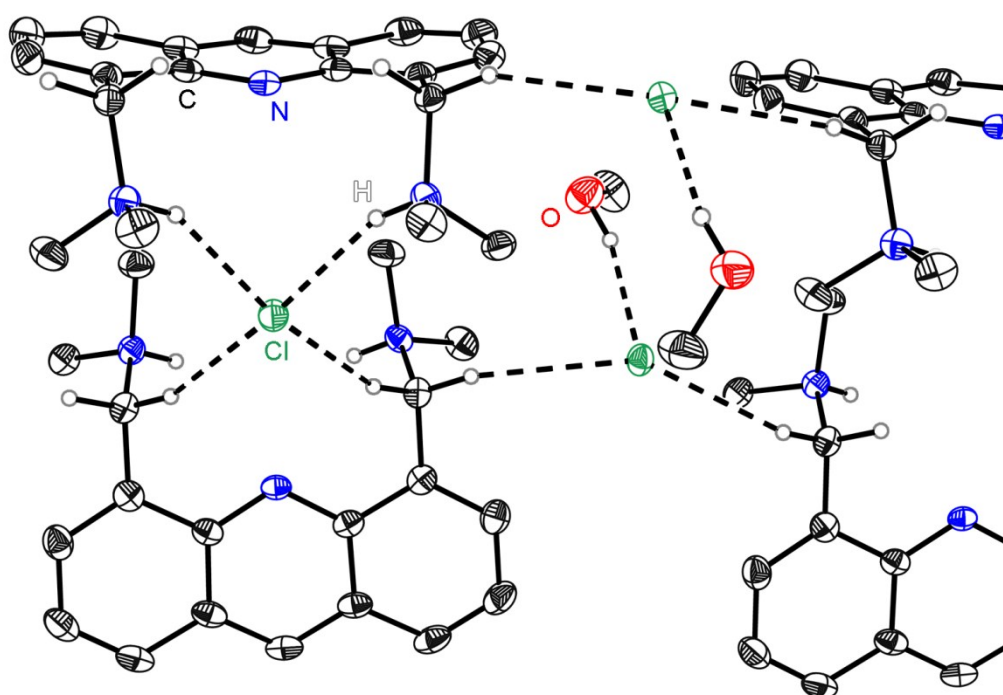
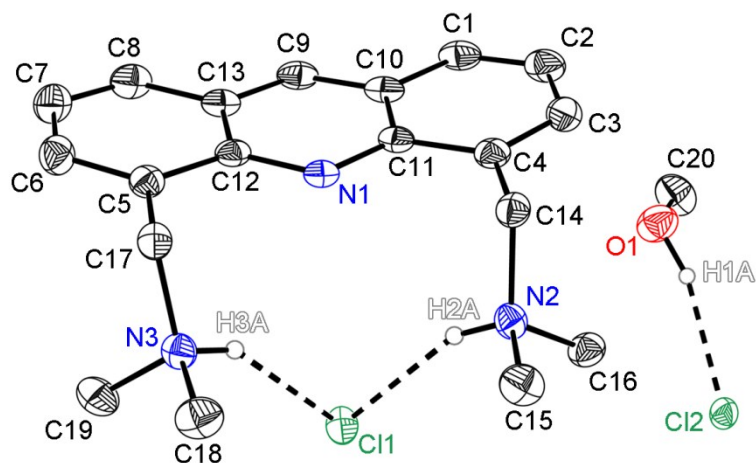


Figure S7.2: Solid state structures of $[(\text{Me}_2\text{NHCH}_2)_2\text{Acr}]\text{Cl}_2 \cdot (\text{MeOH})$ (**6**) with the asymmetric unit (top) and with an illustration of the hydrogen bonds (bottom). The hydrogen atoms of the acridine and of the methyl groups were omitted for clarity. The hydrogen atoms H1A, H2A and H3A are refined freely. Anisotropic displacement parameters are depicted at the 50% probability level. Crystallographic data for compound **6** can be found in Table S7.4. Selected bond lengths, angles and hydrogen bonds will not be discussed here since the completeness of the data set is too low. This was caused by a blockage of the cooling system during the measurement along with the loss of the crystal.

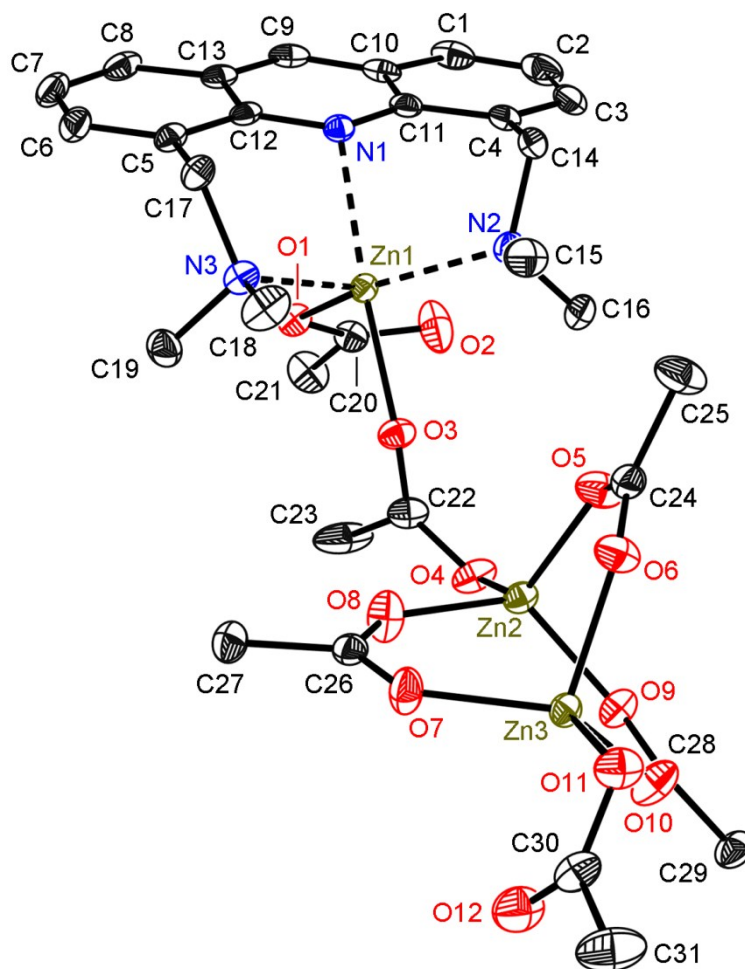


Figure S7.3: Solid state structure of $[\text{Zn}_3(\mu\text{-OAc})_4(\text{OAc})_2(\text{Me}_2\text{NCH}_2)_2\text{Acr}]$ (**7**). All hydrogen atoms were omitted for clarity. Anisotropic displacement parameters are depicted at the 50% probability level.

Table S7.3: Selected bond lengths [pm] and angles [$^\circ$] of **7**.

bond lengths [pm]		angles [$^\circ$]	
N1–Zn1	232.53(14)	N1–Zn1–N2	87.88(5)
N2–Zn1	210.35(15)	N1–Zn1–N3	89.67(5)
N3–Zn1	210.25(15)	N2–Zn1–N3	122.63(6)
O1–Zn1	197.98(12)	N1–Zn1–O3	175.85(5)
O3–Zn1	212.50(12)	N1–Zn1–O1	85.10(5)
O4–Zn2	193.86(13)	O1–Zn1–O3	98.66(5)
O5–Zn2	195.06(13)	C14–N2–C15	106.96(14)
O8–Zn2	194.85(14)	C14–N2–C16	108.27(14)
O9–Zn2	195.76(13)	C15–N2–C16	108.06(15)
O6–Zn3	199.92(13)	C17–N3–C18	107.63(13)
O7–Zn3	195.24(13)	C17–N3–C19	109.37(14)
O10–Zn3	196.61(14)	C18–N3–C19	107.35(14)
O11–Zn3	196.32(12)	C3–C4–C14–N2	–112.06(19)
		C6–C5–C17–N3	110.84(18)

The solid state structures **4a** and **7** have the same zinc coordination motif with three donating nitrogen atoms. The difference between them are the counter anions (Br^- and DMF versus two acetate groups). The N–Zn distances are elongated by 1.16(32) to 2.46(31) pm in the case of **7** which can be explained by the higher Lewis basic character of the acetate oxygen atoms.¹⁷ Therefore, the positive zinc ion is reduced in its charge and is less attractive for the lonepairs of the nitrogen atoms. This weaker bonding situation can additionally be seen by the smaller torsion angles of the amine groups (C3–C4–C14–N2 and C6–C5–C17–N3, respectively).

Table S7.4: Crystallographic data for compound **6** and **7**.

Parameters	6	7
CCDC no.	1423219	1423218
Empirical formula	C ₂₀ H ₂₉ Cl ₂ N ₃ O	C ₃₁ H ₄₁ N ₃ O ₁₂ Zn ₃
Formula weight	398.36 g/mol	843.78 g/mol
Temperature	100(2) K	100(2) K
Wavelength	1.54178 Å	0.56086 Å
Crystal system	Orthorhombic	monoclinic
Space group	<i>Pna2</i> ₁	<i>P2</i> ₁ / <i>c</i>
Unit cell dimensions	<i>a</i> = 16.700(3) Å; α = 90° <i>b</i> = 11.503(2) Å; β = 90° <i>c</i> = 10.836(3) Å; γ = 90°	<i>a</i> = 8.449(2) Å; α = 90° <i>b</i> = 20.113(2) Å; β = 101.42(2)° <i>c</i> = 21.008(3) Å; γ = 90°
Volume	2.0816(6) nm ³	3.4993(11) nm ³
<i>Z</i>	4	4
Density (calculated)	1.271 Mg/m ³	1.602 Mg/m ³
Absorption coefficient	2.905 mm ⁻¹	1.111 mm ⁻¹
<i>F</i> (000)	848	1736
Crystal size	0.10 x 0.10 x 0.05 mm ³	0.179 x 0.168 x 0.122 mm ³
θ range for data collection	28.413 to 66.420°	1.940 to 20.553°
Index ranges	-12 ≤ <i>h</i> ≤ 19, -13 ≤ <i>k</i> ≤ 12, -12 ≤ <i>l</i> ≤ 4	-10 ≤ <i>h</i> ≤ 10, -25 ≤ <i>k</i> ≤ 25, -26 ≤ <i>l</i> ≤ 26
Reflections collected	3602	178761
Independent reflections	1723 [<i>R</i> _{int} = 0.0163]	7163 [<i>R</i> _{int} = 0.0485]
Completeness to θ_{\max}	77.2% ^(a)	99.9%
Absorption correction	Semi-empirical from equivalents	Semi-empirical from equivalents
Max. and min. transmission	0.7528 and 0.6427	0.5599 and 0.5243
Refinement method	Full-matrix least-squares on <i>F</i> ²	Full-matrix least-squares on <i>F</i> ²
Data / restraints / parameters	1723 / 2 / 252	7163 / 0 / 452
Goodness-of-fit on <i>F</i> ²	1.040	1.037
Final <i>R</i> indices [<i>I</i> > 2σ(<i>I</i>)]	<i>R</i> ₁ = 0.0184, w <i>R</i> ₂ = 0.0433	<i>R</i> ₁ = 0.0214, w <i>R</i> ₂ = 0.0526
<i>R</i> indices (all data)	<i>R</i> ₁ = 0.0193, w <i>R</i> ₂ = 0.0436	<i>R</i> ₁ = 0.0252, w <i>R</i> ₂ = 0.0544
Absolute structure parameter	0.008(11)	n/a
Extinction coefficient	n/a	n/a
Largest diff. peak and hole	0.105 and -0.090 eÅ ⁻³	0.646 and -0.458 eÅ ⁻³

(a): The low completeness of the data set is due to a blockage of the cooling system during the measurement along with the loss of the crystal.

8. Computational studies

For the illustration of the difference electron density maps of the following compounds, the electron densities of the individual parts were computed and subtracted from the electron density of the whole complex, respectively. Thereby, the geometry of the atoms is untouched. The individual parts are always the organic ligand **3**, the metal ion (Zn^{2+} / Cd^{2+}), and two methanol molecules or two bromide anions. The regions where the electron density is accumulated due to the interaction of the relevant atoms are illustrated by green density clouds.

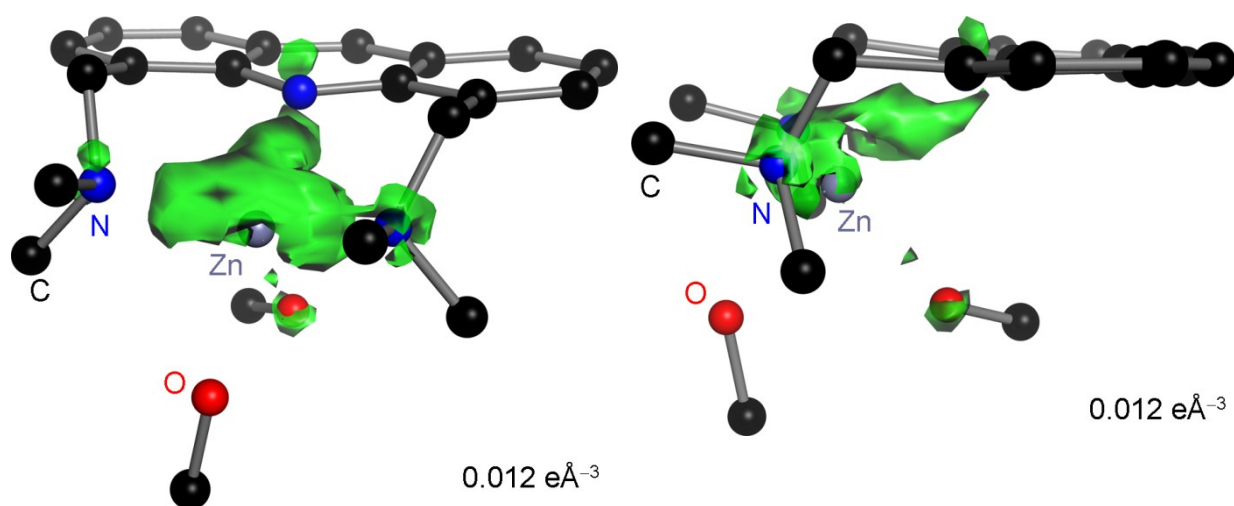


Figure S8.1: Computed difference electron density map of $[(\text{MeOH})_2\text{Zn}\{(\text{Me}_2\text{NCH}_2)_2\text{Acr}\}]^{2+}$ at an isosurface level of $0.012 \text{ e}\text{\AA}^{-3}$ from different perspectives.

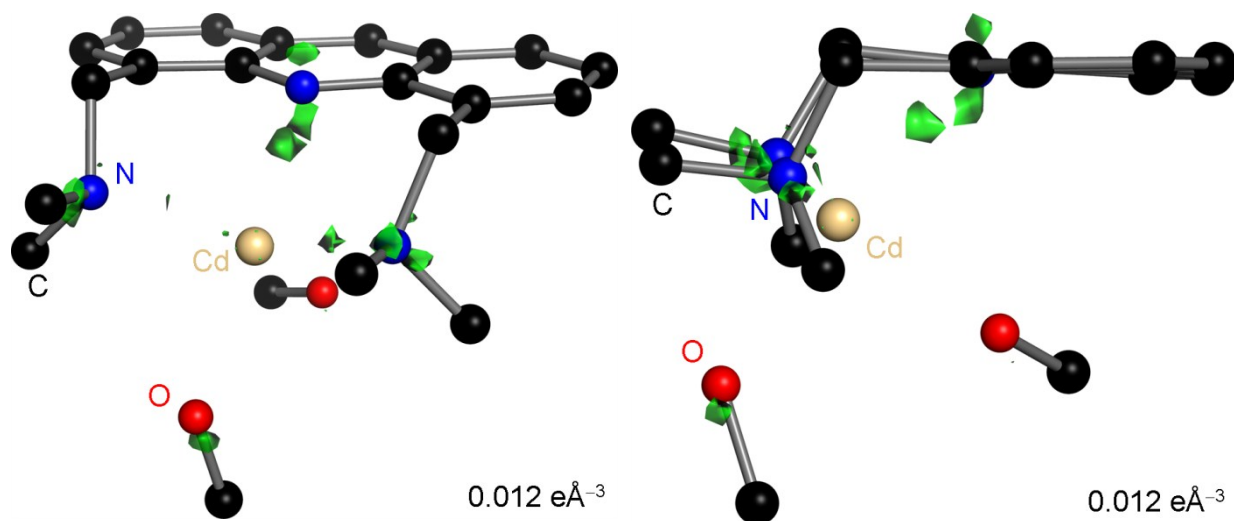


Figure S8.2: Computed difference electron density map of $[(\text{MeOH})_2\text{Cd}\{(\text{Me}_2\text{NCH}_2)_2\text{Acr}\}]^{2+}$ at an isosurface level of $0.012 \text{ e}\text{\AA}^{-3}$ from different perspectives.

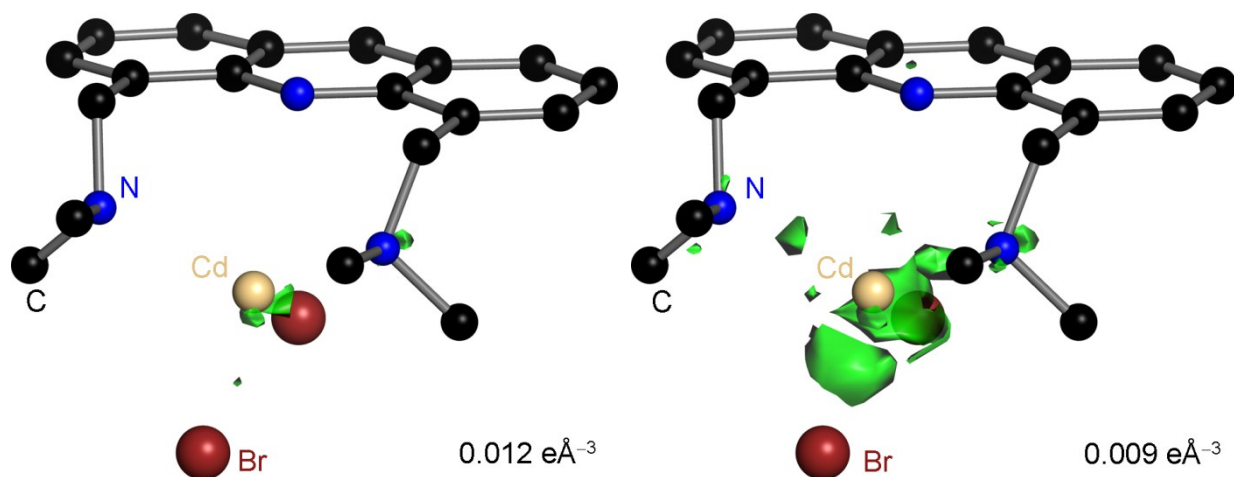


Figure S8.3: Computed difference electron density map of $[\text{CdBr}_2\{(\text{Me}_2\text{NCH}_2)_2\text{Acr}\}]$ (**5**) at an isosurface level of $0.012 \text{ e}\text{\AA}^{-3}$ (left) and $0.009 \text{ e}\text{\AA}^{-3}$ (right).

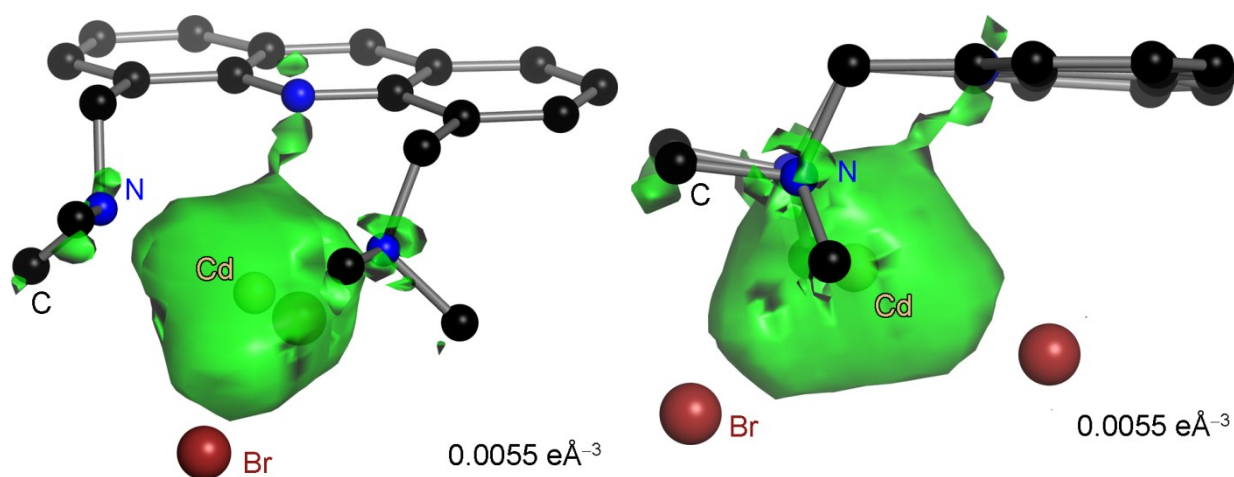


Figure S8.4: Computed difference electron density map of $[\text{CdBr}_2\{(\text{Me}_2\text{NCH}_2)_2\text{Acr}\}]$ (**5**) at an isosurface level of $0.0055 \text{ e}\text{\AA}^{-3}$ from different perspectives.

Table S8.1: NBO second-order perturbation theory analysis of the metal (Zn / Cd) coordination to **3** at the B3LYP-D3/def2-TZVPP level of theory.

	$E^{(\text{PT}2)}$ [$\text{kcal}\cdot\text{mol}^{-1}$]			$d^{(\text{N}-\text{M})}$ [pm]		
	N1	N2	N3	N1	N2	N3
$[(\text{dmf})\text{ZnBr}\{(\text{Me}_2\text{NCH}_2)_2\text{Acr}\}]^+$ (4a)	17.0	25.4	25.1	277.0	221.3	220.1
$[\text{ZnBr}_2\{(\text{Me}_2\text{NCH}_2)_2\text{Acr}\}]$ (4)	5.6	24.7	25.4	---	---	---
$[\text{CdBr}_2\{(\text{Me}_2\text{NCH}_2)_2\text{Acr}\}]$ (5)	4.7	22.8	22.7	283.0	241.7	241.6
$[(\text{MeOH})_2\text{Zn}\{(\text{Me}_2\text{NCH}_2)_2\text{Acr}\}]^{2+}$ (in MeOH)	21.9	25.4	26.5	215.7	207.0	207.0
$[(\text{MeOH})_2\text{Cd}\{(\text{Me}_2\text{NCH}_2)_2\text{Acr}\}]^{2+}$ (in MeOH)	15.0	32.1	31.8	237.3	225.0	225.2

9. References

- (1) (a) Kottke, T.; Stalke, D. *J. Appl. Cryst.* **1993**, *26*, 615-619; (b) Kottke, T.; Lagow, R. J.; Stalke, D. *J. Appl. Cryst.* **1996**, *29*, 465-468; (c) Stalke, D. *Chem. Soc. Rev.* **1998**, *27*, 171-178.
- (2) Schulz, T.; Meindl, K.; Leusser, D.; Stern, D.; Graf, J.; Michaelsen, C.; Ruf, M.; Sheldrick, G. M.; Stalke, D. *J. Appl. Cryst.* **2009**, *42*, 885-891.
- (3) Bruker AXS Inc. *S SAINT v8.30C*, Madison (WI, USA), **2013**.
- (4) Krause, L.; Herbst-Irmer, R.; Sheldrick, G. M.; Stalke, D. *J. Appl. Crystallogr.* **2015**, *48*, 3-10.
- (5) Sheldrick, G. M. *Acta Cryst. A* **2015**, *71*, 3-8.
- (6) Sheldrick, G. M. *SHELXL in SHELXTL v2014/7*, Madison (WI, USA), **2014**.
- (7) Huebschle, C. B.; Sheldrick, G. M.; Dittrich, B. *J. Appl. Cryst.* **2011**, *44*, 1281-1284.
- (8) Müller, P.; Herbst-Irmer, R.; Spek, A. L.; Schneider, T. R.; Sawaya, M. R. *Crystal structure refinement - A crystallographer's guide to SHELXL*. 8th ed.; Oxford University Press: Oxford, 2006.
- (9) (a) Becke, A. D. *Phys. Rev. A* **1988**, *38*, 3098-3100; (b) Lee, C.; Yang, W.; Parr, R. G. *Phys. Rev. B* **1988**, *37*, 785-789; (c) Becke, A. D. *J. Chem. Phys.* **1993**, *98*, 5648-5652; (d) Stephens, P. J.; Devlin, F. J.; Chabalowski, C. F.; Frisch, M. J. *J. Phys. Chem.* **1994**, *98*, 11623-11627; (e) Weigend, F.; Ahlrichs, R. *Phys. Chem. Chem. Phys.* **2005**, *7*, 3297-305; (f) Grimme, S.; Antony, J.; Ehrlich, S.; Krieg, H. *J. Chem. Phys.* **2010**, *132*, 154104-19; (g) Eichkorn, K.; Weigend, F.; Treutler, O.; Ahlrichs, R. *Theor. Chem. Acc.* **1997**, *97*, 119-124.
- (10) (a) Johnson, E. R.; Becke, A. D. *J. Chem. Phys.* **2005**, *123*, 024101; (b) Becke, A. D.; Johnson, E. R. *J. Chem. Phys.* **2005**, *123*, 154101; (c) Johnson, E. R.; Becke, A. D. *J. Chem. Phys.* **2006**, *124*, 174104.
- (11) Andrae, D.; Häußermann, U.; Dolg, M.; Stoll, H.; Preuß, H. *Theor. Chim. Acta* **1990**, *77*, 123-141.
- (12) (a) Foster, J. P.; Weinhold, F. *J. Am. Chem. Soc.* **1980**, *102*, 7211-7218; (b) Reed, A. E.; Weinstock, R. B.; Weinhold, F. *J. Chem. Phys.* **1985**, *83*, 735-746; (c) Reed, A. E.; Curtiss, L. A.; Weinhold, F. *Chem. Rev.* **1988**, *88*, 899-926; (d) Glendening, E. D.; Badenhoop, J. K.; Reed, A. E.; Carpenter, J. E.; Bohmann, J. A.; Morales, C. M.; Weinhold, F. *GenNBO 5.9*. University of Wisconsin: Madison, 2009.
- (13) Neese, F. *WIREs Comput. Mol. Sci.* **2012**, *2*, 73-78.
- (14) (a) Baerends, E. J.; Ellis, D. E.; Ros, P. *Chem. Phys.* **1973**, *2*, 41-51; (b) Whitten, J. L. *J. Chem. Phys.* **1973**, *58*, 4496-4501; (c) Neese, F.; Wennmohs, F.; Hansen, A.; Becker, U. *Chem. Phys.* **2009**, *356*, 98-109.
- (15) (a) Bondi, A. *J. Phys. Chem.* **1964**, *68*, 441-451; (b) Neufeld, R.; Stalke, D. *Chem. Sci.* **2015**, *6*, 3354-3364.
- (16) Karplus, M. *J. Am. Chem. Soc.* **1963**, *85*, 2870-2871.
- (17) Jensen, W. B. *The Lewis Acid-Base Concepts. An Overview*. John Wiley & Sons: New York, 1980.